Geophys. J. Int. (2002) **149,** 422–439

Phase transitions and heat conduction in post-glacial rebound

M. E. Tamisiea* and J. M. Wahr

Department of Physics and Cooperative Institute for Research in Environmental Sciences, CB 390, *University of Colorado, Boulder, CO* 80302, *USA.*
E-mail: tamisiea@sphere.physics.utoronto.ca

Accepted 2001 November 16. Received 2001 November 5; in original form 2001 March 20

SUMMARY

We have developed a method for including phase boundary conditions into post-glacial rebound models that allows for conduction of latent heat away from the boundary. This method returns the chemical boundary results if latent heat conducts away from the phase boundary too slowly to allow the transition to proceed, as is commonly argued. This is not necessarily the case, however. For example, the secular change of the geoid and the vertical uplift rates for phase boundaries with latent heat conduction can differ from the chemical boundary results by up to 10 and 15 per cent, respectively. When modelling the phase transition, we consider two scenarios: the latent heat is released either at a narrow boundary that separates the two phases or over a thick mixed region of the two phases. In the case where the phase transition occurs over a thick enough region (5–10 km), the final results are close to the results obtained by considering a phase boundary that ignores the release of latent heat completely. This thick boundary formulation also suggest that the phase boundaries could respond nearly instantaneously, changing both the elastic load and body Love numbers. However, we have not considered kinetics, the energetics of the mechanisms of the phase transitions, in this formulation. This work suggests a greater knowledge of the kinetics near equilibrium phase transitions is required. A naive calculation indicates that the kinetics will not be a significant factor for post-glacial rebound but will be a limiting factor for earth tides.

Key words: glacial rebound, mantle discontinuities, phase transitions, thermal conductivity.

1 INTRODUCTION

The geodynamic behaviour of the 670 km and, to a lesser extent, the 400 km seismic discontinuities is an open question. The pressures in laboratory experiments at which phase transitions have been observed in the $(Mg, Fe)_2SiO_4$ system correspond to the pressures in the Earth at which discontinuities in seismic velocities occur (e.g. Jackson & Rigden 1998). Thus, the 400 and 670 km boundaries are believed to be caused by phase transitions from olivine to wadsleyite (β-spinel) and ringwoodite (γ-spinel) to perovskite plus magnesiowüstite, respectively. In this system, the entire mantle should be able to mix. However, some believe that the upper and lower mantles are separate reservoirs and little mixing occurs across the boundary (Anderson 1989; Gasparik 1993). These two endpoint views have different implications for the long-term dynamics of the Earth. Convection models must consider these phase transitions explicitly in order to determine the style of mantle convection (e.g. Christensen & Yuen 1985). Nevertheless, for shorter timescale geophysical processes, such as post-glacial rebound (PGR), the possible movement of material between the reservoirs is generally not considered.

The introduction of phase boundaries into PGR models has been studied previously. The first consideration of this problem was by Gjevik (1972), who investigated phase changes as the primary mechanism for motion at the surface. He solved the heat equation to determine changes in density but ignored any other means of material motion. In a similar calculation, O'Connell (1976) showed that the change in density arising from the phase transitions could account for at most about 10–20 per cent of the displacement observed at the surface of the Earth. Thus, the phase transitions could not be the main mechanism for PGR. O'Connell also demonstrated that the response time caused by thermal conduction is 4.5 Myr for the olivine-to-wadsleyite transition and therefore argued that the transitions were unimportant for the loading problem on the timescale of PGR. In response to this article, Christensen (1985) showed that if the boundary is divariant, the phase change occurs over a range of pressures owing to a binary mineral system, it could respond on much shorter timescales. Similarly, Buffett (1993) found analytic solutions that indicated a mixed phase region would respond more quickly than a plane boundary separating the two phases. Christensen (1985) also explored the possibility of convection removing the latent heat of reaction away from the boundary if the phase change was univariant. These early studies, however, ignored the mechanical motion associated with the redistribution of mass caused by isostasy and the resulting feedback into the thermal equations.

*Now at: Department of Physics, University of Toronto, 60 St George Street, Toronto, Ontario, Canada M5S 1A7.

More recently, Mitrovica & Peltier (1989) accounted for the phase boundaries by eliminating the relaxation modes associated with buoyancy forces at the internal density discontinuities. As will be discussed further later, the buoyancy modes for the phase boundaries do 'disappear' for certain cases. However, this technique fails to account for changes that occur in the other modes and to the elastic Love numbers. Johnston *et al.* (1997) included the boundary conditions for a phase transition where the latent heat is ignored, equivalent to the BD2 boundary type described below, and their results show that the phase boundaries modify predictions of surface observations by 10–15 per cent. The same boundary conditions have also been included into direct time-domain calculations of PGR by Hanyk *et al.* (1998) with similar results. Johnston *et al.* (1997) also considered the removal of latent heat by convection as suggested by Christensen (1985). This was accomplished by introducing into the boundary conditions a multiplicative factor determined by the thermal parameters and assumed convection rates. Because the time constant for thermal diffusion is longer than 1 Myr, none of these studies considered the explicit conduction of latent heat away from the boundary, believing that it would be negligible at the relatively short timescales of PGR. The implication is that if conduction were the only means of removing the latent heat of transformation away from a boundary, phase transitions would probably not proceed. However, O'Connell (1976) did show that some of the material would change phase when subjected to pressure disturbances on timescales shorter than the thermal diffusion time constant, and Christensen (1985) suggested that the divariant nature of the boundary could help reduce the response time of the phase transitions.

In this paper, we consider how the conduction of heat away from the boundary will affect signals observed at the surface and displacements of the internal boundaries, and we extend the discussion of the behaviour of the buoyancy mode associated with the phase boundary in the case of an equilibrium phase transition (again BD2 below). In the next section we describe the problem and define the terms that we will use in the rest of the paper. Section 3 examines the possible impact of the kinetic mechanisms on the results of this paper. The theory of coupling heat conduction and mechanical motion at a phase boundary is presented in Section 4. Section 5 describes the rheological models and the thermodynamic assumptions. In Section 6 we present the effects of latent heat conduction on the modes, elastic load Love numbers, internal boundary displacements and surface observations. The results are discussed in the final section.

2 DESCRIPTION OF THE PROBLEM

The behaviour of a phase boundary in response to a surface load is quite different from the behaviour of a chemical boundary, as illustrated in Fig. 1. When a glacier forms at the surface, the pressure at depth increases and the material under the load is pushed downwards. For a chemical boundary, the discontinuity in density—which is how we define the boundary—moves with the material and so moves downwards. However, for a phase boundary, the discontinuity wants to occur at some characteristic pressure, which is determined by the temperature. Thus, because the pressure has increased, the boundary must move upwards. Whichever way the boundary moves, there is now an anomalous density contrast under the load. Buoyancy forces act to smooth out the density contrast through viscous flow. The resulting flow for a chemical boundary, however, will be in the opposite direction to that for a phase boundary because the boundary displacements in these two cases are in opposite directions.

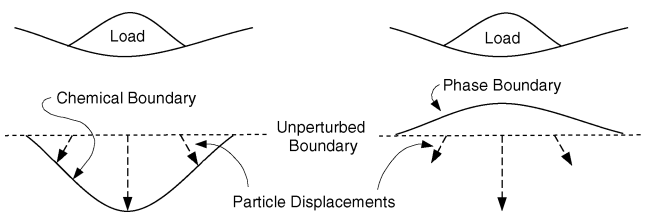

Figure 1. A chemical boundary and a phase boundary have different responses to a load applied at the surface. The density discontinuity, our definition of a boundary, moves with the particles in the case of a chemical boundary. For a phase boundary, however, the location of the phase equilibrium remains at nearly a constant pressure.

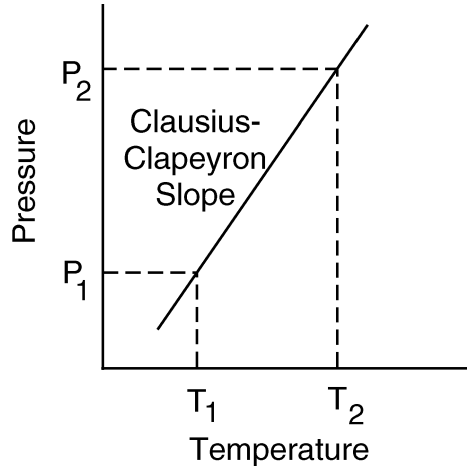

Figure 2. An illustration of the Clausius–Clapeyron slope for the phase change occurring at 400 km depth. An increase in temperature causes the phase transition to occur at high pressures.

The displacement of a phase boundary is not quite this simple because a phase boundary also responds to temperature changes, and there can be temperature changes induced by the load. For example, if the Earth responds adiabatically to the load, then if the pressure increases, so does the temperature. So both P and T increase under the load. Consider the 400 km boundary, where the Clausius–Clapeyron slope $(dP/dT)_c$ is positive. Suppose the temperature increases from T_1 to T_2 as a result of the application of the load. The phase boundary, originally (i.e. when $T = T_1$) at a depth corresponding to P_1, now wants to change phase at a depth corresponding to P_2 (Fig. 2). Because $P_2 > P_1$, the temperature change causes the boundary to move downwards. This temperature effect is smaller than the pressure effect. For example, suppose the load causes the pressure at a depth of 400 km to increase by 4×10^6 Pa (characteristic of the pressure change induced by the addition of the Laurentian ice load). Using the parameter values described in Section 5, we discover that the associated temperature increase would be about 0.04 K. The change in pressure would cause the boundary to move upwards by about 108 m. The change in temperature would cause the boundary to move downwards by about 4 m. So the total displacement would be about 104 m upward. Thus, the adiabatic temperature change only perturbs the results by about 4 per cent in the case of the 400 km boundary.

However, there are two complications. One involves the energy available to change phase, and depends on the kinetics, or mechanisms, of the phase change. We will discuss this in Section 3. The other is that as the boundary moves, material changes phase and

releases (or absorbs) latent heat, which raises (or lowers) the temperature of the boundary and can inhibit the phase change. In the example above, as we load the Earth, the phase boundary wants to start moving upwards in response to the local increase in pressure, but is counteracted slightly by the downward motion in response to the increase in temperature. As the boundary starts to move, material changes phase from the overlying olivine to the underlying wadsleyite. This releases heat and raises the temperature substantially over and above the temperature increase adiabatically related to the change in pressure.

From Fig. 2, we know that a temperature increase causes the boundary to want to change phase back at a higher pressure—and so at a greater depth. The extent to which this inhibits the phase change depends on the latent heat of reaction and on the efficiency with which the material can conduct this heat away from the boundary and thereby minimize its effect on the temperature. This efficiency depends on the thermal conductivity and on the timescale: heat is conducted away more efficiently at longer timescales, and so these effects of latent heat tend to be smaller at longer periods. At short periods, or smaller conductivities, the latent heat release can effectively prevent material from changing phase. In this limit, a phase boundary will move with the material and so will respond as though it were a chemical boundary.

The inhibiting effects of latent heat release are reduced if the phase boundary is not a sharp boundary but is spread out over a kilometre or more. In this case, there is the same amount of total latent heat released as in the thin-boundary case, but now it is spread throughout the boundary region. This results in a smaller temperature increase throughout the boundary region.

In this paper, we consider the phase boundary with several degrees of simplification. In all cases, we assume that the phase boundary remains in equilibrium. That is, if the pressure and temperature conditions cross the line separating the different equilibrium regions, defined by the Clausius–Clapeyron slope, the material will change phase. While the kinetics of the transition may prevent the boundary from remaining in equilibrium, we do not consider this possibility. Given this simplification, there are still many ways to approximate the effect of the latent heat release upon the phase transition. Because a simple one- or two-word description of the boundary types might be misleading, we will refer to them with the abbreviations BD1–BD4. How each of these is modelled mathematically will be described in Section 4.

The boundary type that is most commonly used in PGR studies is a chemical boundary. For a chemical boundary, the constituents on either side of the boundary are different, and the material cannot mix. Thus, a material particle on one side of the boundary will always remain on its original side of the boundary. Therefore, the boundary displacement can be described by the material displacement. We call this boundary BD1.

For phase boundaries, however, material can cross the boundaries. A particle that is initially on one side of the boundary might change phase because of the pressure and temperature perturbation and thus be on the other side of the boundary. This means that the material displacements do not describe the displacement of the boundary. The most simplistic way of incorporating a phase boundary into the formalism is to assume that as soon as the externally induced pressure and temperature perturbations are applied, the material changes phase. This ignores any latent heat release or assumes that it can be conducted away from the boundary infinitely quickly. We will call this type of boundary BD2.

A more realistic way of accounting for the latent heat is to model its conduction away from the boundary. This has the effect of forcing the boundary to react differently on different timescales. If the boundary is forced quickly, the latent heat released does not have time to conduct away from the boundary. Thus the phase transition cannot proceed because the conditions are no longer favourable. However, if the forcing is slower, then the latent heat can escape, and the transition proceeds. The meaning of quickly and slowly above have generally been defined in terms of a heat conduction diffusion time (O'Connell 1976). This type of boundary will be represented by BD3.

Table 1. Summary of the boundary models abbreviated as BD1–BD4.

Boundary abbreviation	Brief description
BD1	A chemical boundary where the boundary moves with the material
BD2	A phase boundary where the latent heat release is ignored
BD3	A phase boundary where the latent heat is released at an infinitely thin boundary
BD4	A phase boundary where the latent heat is released over a thick region

Finally, all of the above boundary types assume that the boundary is infinitely thin and is at a well-defined position. Realistically, the boundaries in the Earth occur over a finite thickness. There are several reasons for this. First, when material flows through the boundary, latent heat is released. This constant release causes the adiabat to follow the Clausius–Clapeyron slope (Verhoogen 1965). This effect is reduced, however, by the conduction of heat away from the boundary (e.g. Jeanloz & Thompson 1983). Secondly, the mineral transitions are divariant and thus should occur over a range of pressures (e.g. Jeanloz & Thompson 1983). Finally, kinetics will play a role in the boundary thickness (e.g. Solomatov & Stevenson 1994). Kinetics will prevent the phase transition from proceeding at its equilibrium position and will increase the radial extent over which the two phases can exist. While we are not modelling the processes that cause the finite thickness to occur, we can model the effect of latent heat being released over a thick boundary instead of an infinitely thin boundary. We will present results for boundaries ranging from 1 to 10 km. The thick boundary improves the possibility that the material will change phase on shorter timescales because less latent heat will be released at a particular position. This type of boundary will be represented by BD4. The four boundary types are summarized in Table 1.

3 KINETICS

Throughout this paper we will assume that material will change phase instantaneously as soon as the values of pressure and temperature cross from one phase region to another. In reality, there is a potential energy barrier that must be surmounted in order for the phase transition to occur, and so there will be no phase change unless the molecules have sufficient kinetic energy. Consequently, the pressure and temperature may have to move well into the region of the new phase before there is enough ambient energy to allow the phase transition to proceed. These energy considerations are usually loosely referred to as the kinetics of the phase transformation.

The importance of kinetics is well known for subducting slabs (e.g. Däßler & Yuen 1996; Kirby *et al.* 1996; Devaux *et al.* 1997). While equilibrium thermodynamics would cause the 400 km boundary to be elevated in a cold descending slab, the kinetics cause the olivine to exist metastably down to depths as great as 720 km (Kirby *et al.* 1996). This metastability is the result of the slab descending faster than the reaction rates allow the material to change phase. The

reaction rates are particularly slow in this case because of the cold temperature of the slab.

The kinetics of the olivine-to-wadsleyite phase transition have been studied in some detail (for a recent summary see Kerschhofer *et al.* 1998), but often in the context of large variations of temperature and pressure, which are useful in modelling subducting slabs. The models of this transformation often assume two types of mechanisms. The first is nucleation where a new phase develops in the middle of the original phase. The second mechanism is interface-controlled growth of one phase at the expense of the other. Both of these mechanisms have a region in pressure and temperature space (which for our study can be transferred to real space using the hydrostatic pressure gradient and the adiabatic temperature gradient) near the equilibrium position of the boundary where they are inhibited from occurring because it is not energetically favourable for the material to change phase. The distance from these equilibrium conditions is larger for nucleation than for growth (Rubie 1993; Kirby *et al.* 1996). When investigating subduction, one must consider both of these mechanisms because the phase boundary in a subducting slab is far from the equilibrium conditions. However, of these two mechanisms, growth is more likely to dominate in our case because we are investigating relatively small perturbations of the boundary from its equilibrium position. One should note that a third mechanism, diffusion, may dominate for these near-equilibrium processes and probably governs the ringwoodite to perovskite plus magnesiowüstite transition (Rubie 1993). In the discussion that follows, though, we explore growth because the kinetic parameters for this process are better known.

To obtain an estimate of the impact of kinetics, we compare the growth rate with the velocity of the boundary caused by PGR. If the velocity of the boundary is sufficiently greater than the growth rate of the new phase, then one can ignore the phase transition and assume that the density discontinuity behaves as a chemical boundary. While temperature effects dominate the kinetic rates in the case of cold subducting slabs, the energy difference between the two phases dominates for PGR because the perturbations occur from the equilibrium position of the boundary. A phase transition would not proceed unless a geophysical process introduces an energy difference between the two phases. We assume that the energy difference caused by PGR is equal to the change in pressure caused by the boundary moving through the hydrostatic pressure gradient times the transformational change in volume. Using this value along with parameters for the olivine-to-wadsleyite transition from Rubie & Ross (1994) in the growth rate equation (see Kirby *et al.* 1996, eq. 1), we find that the estimated growth rate of the new phase is two orders of magnitude larger than the velocity of the boundary. Thus, if the growth were the appropriate mechanism for describing the phase transformation under the conditions caused by PGR, then kinetics would not be a significant factor.

As will be shown in Section 6.2, we are also interested in the impact of kinetics on other geophysical processes, such as earth tides. Using the same processes for an earth tide with a period of 1 day, we find the growth rate of the phase transition to be several orders of magnitude smaller than the velocity of the boundary. In this case kinetics would prohibit the phase change. However, both of these results should be viewed with caution in that diffusion may be the dominant kinetic process. Diffusion of atoms is generally a slower process than that of rearrangement (growth or nucleation). Transitions governed by this mechanism might be helped by longer timescales because diffusion has an explicit dependence upon time, whereas the proceeding argument depends only on the perturbation from the equilibrium pressure. We believe that the results that follow, particularly for the elastic Love numbers, warrant a more careful examination of the kinetic mechanisms governing these small-amplitude motions.

4 THEORY

The process of simultaneously solving the momentum equation, the constitutive equation, and Poisson's equation in the context of PGR is well described in the literature (e.g. Wu & Peltier 1982). One generally transforms the equations into the Laplace domain, with transform variable s, and expands the equations in terms of spherical harmonics. Certain values of s, associated with natural decay times of the system, are called modal frequencies, and the corresponding relaxation states are called modes. The most important of these are the buoyancy modes, which are related to the gravitational restoring force caused by the displacement of a density discontinuity. For the Earth model described in the next section, these modes are denoted by M0, associated with the surface; L0, associated with the lithosphere–mantle interface; C0, associated with the core–mantle interface; M1, associated with the 670 km boundary; and M2, associated with the 400 km boundary. Surface observations mostly reflect the excitation of M0, though L0 and C0 also contribute strongly at low angular degrees (long wavelengths). The M1 and M2 modes contribute more at low degrees than at high degrees (though their contributions to surface observations are relatively small in any case).

In a given layer in the mantle, following Wu & Peltier (1982), the differential equations can be written as

$$\frac{d\mathbf{y}}{dr} = \mathbf{A}\mathbf{y}, \tag{1}$$

where $\mathbf{A}$ is a matrix and $\mathbf{y}$ is the six-component vector $(U, V, T_r, T_\theta, \Phi, Q)^{\mathrm{T}}$, consisting of the radially dependent coefficients of the spherical harmonic decompositions of radial and horizontal displacements (U and V), radial and horizontal stress components (T_r, T_θ), and Eulerian potential and modified gravitational acceleration scalars (Φ, Q). A subscript l, indicating the degree, is assumed on each of the variables. The load Love numbers (the radial, h_l, horizontal, ℓ_l, and gravitational, k_l, response of the Earth to a point load in both time and space) can be related to U, V and Φ, respectively (e.g. Wu & Peltier 1982). In the case of BD1 conditions, all of the above variables are continuous across the boundary. However, that will not be the case for a phase boundary.

Using the conservation of mass, one can derive the boundary condition for a phase boundary, BD2–BD4. Fig. 3 illustrates a Gaussian pillbox argument that the mass leaving the box minus the mass entering is equal to the change of mass in the box. As the left- and right-hand sides of the box become vanishingly small, flow through those sides do not contribute to the change in mass. The only mass that does contribute flows through the top and bottom of the box, and this argument reduces to

$$\rho_+ u_{r+} - \rho_- u_{r-} = (\rho_+ - \rho_-)\delta r, \tag{2}$$

where u_r is the radial displacement of a particle at the boundary, and δr, the radial phase boundary displacement, is given by

$$\delta r = \frac{\delta P - (dP/dT)_c \delta T}{\rho g + (dP/dT)_c (dT_o/dr)}, \tag{3}$$

where dT_o/dr is the background temperature profile (Dehant & Wahr 1991; Defraigne *et al.* 1996). The Eulerian perturbations in temperature and pressure, δT and δP, can be related to the solution scalars for stress and displacement. The way in which δT is related

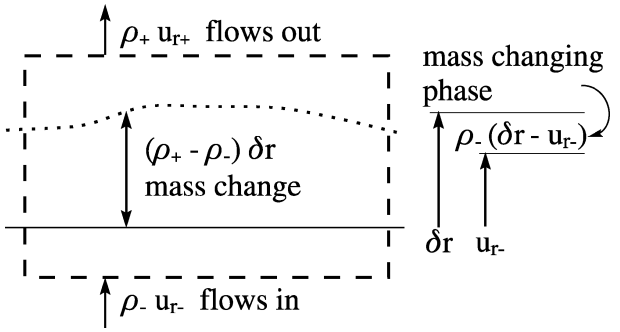

Figure 3. A Gaussian pillbox (dashed box) near the boundary showing the conservation of mass. The solid line represents the unperturbed boundary and the dotted line is the perturbed boundary. The two arrows right of the pillbox show the displacement, $u_{r\_}$, of a particle that was just below the boundary before the perturbation, and the displacement of the boundary itself, δr. The density, ρ_-, times the difference between these two displacements gives the mass of material that changes phase.

to these solutions depends on the boundary type (BD2–BD4). Note that if the boundary moves with the particles (the BD1 case), then $\delta r = u_r$ and eq. (2) reduces to $u_{r+} = u_{r-}$, as expected for a chemical boundary.

A general reference for the following thermodynamic relationships is Anderson (1989). From the equation of state δT can be related to $\delta\rho$ and δP by

$$\frac{\delta\rho}{\rho} = -\alpha\delta T + \frac{\delta P}{k_T}, \tag{4}$$

where α is the coefficient of thermal expansion and k_T is the isothermal bulk modulus. If one assumes that the relationship between δT and $\delta\rho$ is adiabatic, then

$$\frac{\delta\rho}{\rho} = \frac{1}{\gamma T}\delta T, \tag{5}$$

where γ is the Grüneisen parameter, and δT can be expressed as

$$\delta T = \frac{\alpha T}{\rho c_P}\delta P, \tag{6}$$

where c_P is the heat capacity at constant pressure. It is interesting to note that if dT_o/dr is also assumed to be adiabatic, i.e.

$$\frac{dT_o}{dr} = -\rho g\frac{\alpha T}{\rho c_P}, \tag{7}$$

then eqs (3) and (6) reduce to

$$\delta r = \frac{\delta P}{\rho g}. \tag{8}$$

Thus, in this case the response of the boundary is effectively decoupled from the background temperature gradient and is independent of the temperature perturbation. The boundary simply moves through the background pressure field to exactly offset any changes caused by the externally applied pressure. Eq. (8) is used by Johnston *et al.* (1997). Note that eq. (7) states that the background, unperturbed Earth is adiabatic, which may or may not hold (we always assume this holds in the numerical calculations below), whereas eq. (6) states that the relationship between the perturbed T and P is adiabatic, which is likely to always be true as long as there is no release of latent heat. Therefore, it is reasonable to expect that eq. (8) can be used to describe BD2 conditions. The additional contribution from latent heat release will be described below. Finally, one needs to relate δP, the Eulerian quantity used in eqs (3) and (4), to the solution scalars of eq. (1). δP is given by

$$\delta P = -\frac{1}{3}\text{trace}\,\overleftrightarrow{\tau} + \rho g u_r, \tag{9}$$

where $\overleftrightarrow{\tau}$ is the stress tensor (e.g. Dahlen & Tromp 1998).

One can perform a spherical harmonic expansion of eqs (2), (3), and (9) in order to express these equations in terms of the scalar quantities used in eq. (1). This gives

$$\rho_+ U_+ - \rho_- U_- = (\rho_+ - \rho_-)\delta R, \tag{10}$$

where δR is the spherical harmonic coefficient of δr,

$$\delta R = \frac{\delta P_l - (dP/dT)_c\delta T_l}{\rho g + (dP/dT)_c(dT_o/dr)}, \tag{11}$$

δT_l is the spherical harmonic coefficient of δT, and

$$\delta P_l = -\frac{\bar\gamma}{3\mu}T_r + \left(\rho g - \frac{4\bar\gamma}{3r}\right)U + \frac{2\bar\gamma l(l+1)}{3r}V, \tag{12}$$

where $\bar\gamma = \mu(3\lambda + 2\mu)/(\lambda + 2\mu)$. Thus, the BD2 conditions are obtained using eqs (10)–(12) and deriving δT_l from the spherical harmonic expansion of eq. (6).

When latent heat is released from either a narrow or thick boundary, BD3 or BD4 conditions, its effects on δT_l need to be included by modelling the conduction of heat away from the boundary. We assume that the change in temperature, δT, consists of two parts: an adiabatic portion given by eq. (6) and a portion, θ, which results from the release of latent heat. In order to calculate θ we consider a simple spherical, two-layer Earth model. The heat equation is given by

$$\nabla^2\theta = \frac{\rho c_P}{k}\dot\theta, \tag{13}$$

where k is the conductivity and the overdot is a partial time derivative. The boundary conditions at the internal discontinuity, where the latent heat is released, are

$$\theta_+ = \theta_- \tag{14a}$$

$$\partial_r\theta_- - \partial_r\theta_+ = \frac{Q}{k} = \frac{\rho_- L}{k}(\dot\delta r - \dot u_{r\_}) \tag{14b}$$

where Q is the rate of latent heat released per unit area at the interface and k is assumed to be the same on either side of the boundary (Özişik 1993). The second equality in eq. (14b) expands Q in terms of L, the latent heat per mass required to change the phase of material below the boundary into material above the boundary (Schubert *et al.* 1975). The factor $\dot\delta r - \dot u_{r\_}$ represents the rate of change of the thickness of material that has changed phase (see Fig. 3). For both the 400 and 670 km boundaries, L has the same sign as the Clausius–Clapeyron slope. The final set of boundary conditions is that θ goes to zero at both the Earth's centre and outer surface. These assumptions are justified by the fact that this temperature perturbation falls off quickly away from the boundary.

The Laplace transforms of eqs (13) and (14), after transforming to spherical harmonic coefficients, are

$$\frac{1}{r^2}\frac{\partial}{\partial r}\left(r^2\frac{\partial\theta_l}{\partial r}\right) = \left[\frac{s\rho c_P}{k} + \frac{l(l+1)}{r^2}\right]\theta_l \tag{15}$$

and

$$\theta_{l+} = \theta_{l-} \tag{16a}$$

$$\partial_r\theta_{l+} - \partial_r\theta_{l-} = \frac{s\rho_- L}{k}(U_- - \delta R). \tag{16b}$$

The solutions to eq. (15) are spherical Bessel functions of the form $j_l(\sqrt{|s|/\kappa}r)$ and $y_l(\sqrt{|s|/\kappa}r)$ if s is negative and $i_l(\sqrt{s/\kappa}r)$

and $k_l(\sqrt{s/\kappa}r)$ if s is positive where $\kappa = k/(\rho c_P)$ is the thermal diffusivity.

Using the modal method typically used to invert the solution to the time domain would give an infinite number of modes (all with negative values of s) owing to the oscillation of the Bessel functions j_l and y_l when s is negative. Very few, if any, of those thermal modes would be important when summed together to obtain the deformation. Instead, the principal effect of those modes is that they can act to obscure the more important buoyancy modes (i.e. M0, L0, etc.) during the root-finding procedure. In the range of s values where the buoyancy modes occur for BD1 conditions, the Bessel functions oscillate rapidly owing to large arguments. These BD1 modes would presumably be the most important modes for the models with thermal conduction as well, but there they would be obscured by the effects of the oscillating j_l and y_l. Thus, for the boundaries that include latent heat release we resort to the collocation technique, which uses only positive s values, to perform the inverse Laplace transform (e.g. Peltier 1974; Mitrovica & Peltier 1992). This has the disadvantage of not allowing one to track the behaviour of specific, physically significant modes, but it does allow one to include the contributions of all of the modes.

Assuming that all of the heat is released at a thin boundary (BD3 conditions) in a two-layer Earth model, the solutions for θ_l are

$$\theta_l(r) = \frac{\rho_- Ls}{k}\zeta b^2 I_l(b, r)\,(U_- - \delta R) \quad r \le b \tag{17a}$$

$$\theta_l(r) = \frac{\rho_- Ls}{k}\zeta b^2 I_l(r, b)\,(U_- - \delta R) \quad r \ge b, \tag{17b}$$

where

$$I_l(x_1, x_2) = \frac{[i_l(\zeta x_1)k_l(\zeta a) - i_l(\zeta a)k_l(\zeta x_1)]\,i_l(\zeta x_2)}{i_l(\zeta a)}, \tag{18}$$

a is the radius of the Earth, b is the radius of the phase boundary and $\zeta = \sqrt{s/\kappa}$. If we define θ_{lo} through the equation

$$\theta_l(b) = \theta_{lo}(U_- - \delta R) \tag{19}$$

and assume both that the Earth is incompressible ($\lambda \to \infty$ so that $\bar{\gamma} \to 3\mu$) and dT_o/dr is adiabatic (see eq. 7), then one can combine eqs (6), (10)–(12) and (19) to obtain

$$U_+ = U_- - \frac{(\rho_+ - \rho_-)}{\rho_+}\frac{Z_o}{D - (dP/dT)_c\,\theta_{lo}} \times \left[T_{r_-} + \frac{4\mu}{b}U_- - \frac{2\mu l(l+1)}{b}V_-\right], \tag{20}$$

where

$$D = \rho g Z_o = \rho g + \left(\frac{dP}{dT}\right)_c \frac{dT_o}{dr}. \tag{21}$$

If one also assumes that $\theta_{lo} = 0$ (no heat released from the phase transformation), then eq. (20) further reduces to

$$U_+ = U_- - \frac{(\rho_+ - \rho_-)}{\rho_+}\frac{1}{\rho_- g}\left[T_{r_-} + \frac{4\mu}{b}U_- - \frac{2\mu l(l+1)}{b}V_-\right] \tag{22}$$

which agrees with eq. (28) in Johnston *et al.* (1997) and is the equation we use for our BD2 conditions.

For BD4, the latent heat release is spread over a thick region as discussed in the introduction. To model this we introduce a function, $n(x', t')$, which gives the fraction of material at radius x' and time t' that is in the same phase as the material above the boundary region. Thus, $n(x', t')$ varies from 0 below the boundary to 1 above the boundary and is centred at radius $x_p(t')$ (i.e. $n(x_p(t'), t') = 1/2$), chosen to be the radius where the pressure and temperature conditions satisfy the Clausius–Clapeyron equation at time t'. We choose x' and $x_p(t')$ to be Lagrangian coordinates (i.e. coordinates attached to material particles), so that if the boundary moves with the material particles then $x_p(t')$ and $n(x', t')$ do not change. We choose an ad hoc form for $n(x', t')$ that has most of the phase change occurring near $x_p(t')$ and that has a time derivative that is easy to integrate over x' (see below):

$$n(x', t') = \mathrm{erfc}[(x_p(t') - x')/w]/2, \tag{23}$$

where w is the half-width of the boundary. As an example, if the boundary is 4 km thick, so that $w = 2$ km, then $n(x', t')$ increases by 0.84 in a 4 km region centred about $x_p(t')$. Note that the shape of the distribution will not change with time but that the central radius, described by $x_p(t')$, will. The latent heat release comes from the change in the position of this distribution with time

$$\dot{n}(x', t') = -\dot{x}_p(t')\frac{e^{-[x_p(t') - x']^2/w^2}}{\sqrt{\pi}\,w}. \tag{24}$$

Examples of both $n(x', t')$ and $\dot{n}(x', t')$ are shown in Fig. 4. Because $x_p(t')$ is the Lagrangian coordinate of the centre of the phase boundary region, we can set $\dot{x}_p(t') = \dot{\delta}r - \dot{u}_{r_-}$ in eq. (24) (see Fig. 3).

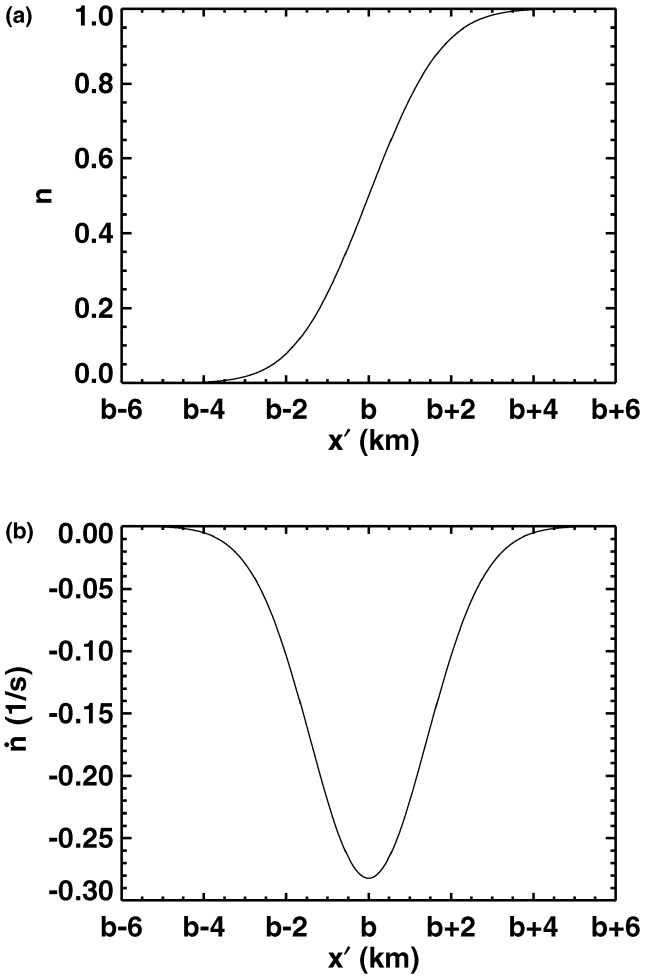

Figure 4. The functions (a) $n(x', t')$ and (b) $\dot{n}(x', t')$ as a function of position. The function $n(x', t')$ gives the fraction of the material that is in the same phase as the material above the boundary region. For these plots, the position of the phase boundary, $x_p(t')$, equals b, the boundary is 4 km thick, and $\dot{x}_p(t') = 1$ km s^{-1}.

To find the temperature perturbation caused by this change $\dot{n}(x', t')$ in the phase concentration, we decompose the phase boundary region into infinitesimally thin layers, find the temperature perturbation caused by the phase transformations that occur in each of the thin layers, and add together (integrate) these temperature perturbations. For example, suppose we want to find the temperature perturbation at x caused by the phase transformations in the infinitesimal layer of thickness dx' at x'. The rate at which latent heat is released per unit area at x' (i.e. Q in eq. 14) is equal to the latent heat per mass, L, required to change material below the boundary into material above the boundary, multiplied by the rate at which mass per area is transformed from material above the boundary into material below the boundary. For our thin layer at x', the rate of mass transformation between these phases is $-\rho_- \dot{n}(x', t')\, dx'$. Thus, the latent heat released by the layer is

$$Q = -\rho_- L \dot{n}(x')\, dx' = \rho_- L(\dot{\delta r} - \dot{u}_{r-}) \frac{e^{-[x'-x_p(t')]^2/w^2}}{\sqrt{\pi} w}\, dx'. \qquad (25)$$

To simplify the integration over the thin layers, we assume that $x_p(t') = \text{constant} = b$ in the exponential factor of eq. (25), where b is the radius of the equilibrium position of the centre of the boundary region. This is equivalent to assuming that the rate of change of the distribution will not move with the boundary so that the maximum temperature perturbation will always be at the equilibrium position of the boundary. Because the temperature perturbation that goes into the boundary conditions, through θ_{lo} in eq. (20), is measured at the equilibrium position of the boundary, that temperature perturbation and thus the effect of latent heat release on the boundary displacement are overestimated. Therefore, if anything, this approximation tends to underestimate the total effect of phase transitions on the PGR process. However, this effect should be small as long as the square of the error in the position of the boundary, say $(\delta b)^2$, is small compared with w^2. After making this approximation for $x_p(t')$, expanding Q in spherical harmonics, and taking the Laplace transform, we find that for this thin layer at x' the boundary condition (eq. 16b) is replaced by

$$\partial_r \theta_{l+} - \partial_r \theta_{l-} = \frac{s\rho_- L}{k}(U_- - \delta R) \frac{e^{-(x'-b)^2/w^2}}{\sqrt{\pi} w}\, dx'. \qquad (26)$$

Thus, the temperature perturbation at r owing to the phase transformation in the thin layer at x', is given by eq. (17) with x' replacing b and multiplying the right-hand sides of eq. (17) by $e^{-(x'-b)^2/w^2}\, dx'/\sqrt{\pi} w$.

Using this result, one can integrate this modified form of eq. (17) over x' to find the temperature at r owing to material changing phase everywhere in the boundary region. This temperature profile is given by

$$\theta_l(r) = \frac{\rho_- L s}{k}(U_- - \delta R)\left[\int_0^r \zeta x'^2 I(x', r) \frac{e^{-(x'-b)^2/w^2}}{\sqrt{\pi} w}\, dx' + \int_r^a \zeta x'^2 I(r, x') \frac{e^{-(x'-b)^2/w^2}}{\sqrt{\pi} w}\, dx'\right]. \qquad (27)$$

If θ_{lo} is again defined (see eq. 19) as the factor multiplying the term $(U_- - \delta R)$ in eq. (27), then the boundary condition for U has the same form, eq. (20), as it does for BD3 conditions. One should note that this θ_{lo} will always be smaller than θ_{lo} obtained for a thin boundary, because the total heat content of the phase change is released over a wider region.

Finally, as mentioned earlier, we use a collocation technique to perform the inverse Laplace transform. As a check of this method we compare the modal solutions with the collocation solutions for the BD1 and BD2 models. The collocation technique gives solutions that are virtually identical to those from the modal technique when sampling is at five points per decade (ppd) over 11 decades, 10^{-17}–10^{-6} s^{-1}, a larger number of points than used by Mitrovica & Peltier (1992). While this range may seem unnecessarily large when sampling the Love number spectrum to obtain surface displacements, the spectrum for internal boundary displacements has a significant power spread over a greater number of decades than does the spectrum for outer surface displacements. We have found that the addition of conductivity to the problem, as required for the BD3 and BD4 conditions, also causes the function to vary over more decades.

Once conductivity is added, a general check of the method can be performed by looking at the limits of the conductivity. If the value of conductivity is very small, then the latent heat would not be able to diffuse out of the region. If the heat cannot escape, the phase transition will not be able to proceed, and the boundary response should be equivalent to that of the BD1 conditions. If the value is very large, the latent heat diffuses quickly away from the boundary. Thus, one can essentially ignore the latent heat, and the boundary response should be close to that of the BD2 conditions. For the low-conductivity limit, we divide the conductivities of both boundaries by 10^5, and the corresponding solution is indistinguishable from the BD1 modal solution. For the high-conductivity limit, we multiply the conductivities by 10^{10} and sample the Love number spectrum at 5 ppd from 10^{-17} to 10^4 s^{-1}. The larger range is needed in this particular case because the thermal modes cause a variation in the spectrum at larger values of s. As will be discussed in Section 6.2 the elastic load Love numbers are different for BD2 and BD3 conditions, and when these differences are taken into account, the resulting collocation solution is identical to the BD2 modal solution.

5 RHEOLOGICAL AND THERMODYNAMICAL MODELS

Because we are only interested in the general effects of introducing phase boundaries into the formalism, we use a five-layer incompressible Earth model, listed in Table 2, which has been used in a previous study of PGR (Han 1993). This model includes an inviscid core and a 120 km thick elastic lithosphere. Four models of viscosity that assume a single discontinuity at the 670 km boundary are also included in Table 2. The various viscosity jumps across the 670 km boundary represent a variety of views concerning the viscosity profile, where some studies find a small jump (e.g. Tushingham & Peltier 1992) and other studies find a large jump (e.g. Nakada & Lambeck 1989). There are also some indications that the value of the viscosity in the upper mantle may be smaller than 10^{21} Pa s, the value that has been assumed classically (e.g. Nakada & Lambeck 1989). For that reason, Models 2 and 4 have the same lower-mantle viscosity but have a factor of 2 difference in upper-mantle viscosity.

Table 2. Rheology models.

Depth (km)	v_s (km s^{-1})	ρ (kg m^{-3})	ν (10^{21} Pa s) Model number			
			1	2	3	4
6371–2891	0.0	10 925	0.0	0.0	0.0	0.0
2891–670	6.6	4970	2.0	5.0	20.0	5.0
670–400	5.25	3850	1.0	1.0	1.0	0.5
400–120	4.33	3070	1.0	1.0	1.0	0.5
120–0	4.33	3070	∞	∞	∞	∞

We use ICE-3G (Tushingham & Peltier 1991) as our ice model for the deglaciation phase. The glaciation phase is modelled so that its spatial dependence is identical to the starting distribution in ICE-3G and is grown continuously for the 90 kyr prior to the start of ICE-3G. If more than one loading cycle is used, we simply repeat the loading cycle.

Unlike in most PGR studies, the inclusion of phase boundaries requires that we adopt numerical values for thermal parameters. We assume that the mantle consists of olivine, wadsleyite (β-spinel), ringwoodite (γ-spinel) and perovskite plus magnesiowüstite in successively deep layers. It is commonly believed that the phase transitions between these minerals contribute strongly to the 400 and 670 km discontinuities. Because there is no boundary in our rheology model at 520 km, the effect of the possible phase transition from wadsleyite to ringwoodite is not included. These minerals probably only make up 40–60 per cent of the mineralogy of the mantle (e.g. Jackson & Rigden 1998). While the rest of the minerals that make up the mantle probably contribute significantly to the nature of these boundaries (e.g. Gasparik 1990; Vacher *et al.* 1998), this model will give one an idea of how phase transitions can affect the final results.

We need to adopt values for: the Clausius–Clapeyron slopes, $(dP/dT)_c$; the heat capacity, c_P; the thermal expansivity, α; the temperature, T; and the conductivity, k. The values for c_P and α are obtained from the equations given in Saxena (1996). The values of k are derived from Hofmeister (1999), which include both lattice and radiative contributions. We correct both k and α for temperature and pressure, whereas we correct c_P only for temperature, because the effect of pressure is only expected to be around 10 per cent (Anderson 1989). The temperature at 670 km is from Ito & Katsura (1989) and the adiabatic temperature gradient, eq. (7), is used to obtain the value at 400 km. The values of the Clausius–Clapeyron slopes are chosen to be within a range found by experiment (Bina & Helffrich 1994). The parameters that go into the boundary condition need to be evaluated on only one side of the boundary (Dehant & Wahr 1991). For example, while we use $\rho_-(\delta r - u_{r-})$ to represent the mass of material that changed phase, we could have used the quantity $\rho_+(\delta r - u_{r+})$. Because we use the first expression, we choose to use values of thermal and rheological parameters from the lower side of the boundary in the various boundary equations unless other values are specified explicitly, such as in the expressions for $\Delta\rho$ or the conservation of mass (eq. 2). We then derive the diffusivity, κ, and the latent heat release, L, using the formulae

$$\kappa = \frac{k}{\rho_- c_P} \tag{28}$$

and

$$L = \frac{\Delta\rho T}{\rho_- \rho_+}\left(\frac{dP}{dT}\right)_c, \tag{29}$$

where the last equation is taken from Schubert *et al.* (1975). For κ we use the densities listed in Table 2. To estimate the latent heat, however, we take values for the densities and for the boundary density jumps from PREM (Dziewonski & Anderson 1981). The rheology model listed in Table 2 adopts the average properties for an entire layer, and thus its density jumps across boundaries are unrealistic. Table 3 shows the values of assumed and derived thermodynamic properties. To take into account the uncertainties of these values, we both increase and decrease the value of k by an order of magnitude as liberal estimates to determine the sensitivity of the results to this parameter.

Table 3. Thermal parameters.

Parameter	Value		
	400 km	670 km	Units
	Assumed values		
T	1753	1873	K
k	2.93	7.39	W m^{-1} K^{-1}
α	2.76×10^{-5}	2.96×10^{-5}	K^{-1}
c_P	1.315×10^3	1.34×10^3	J kg^{-1} K^{-1}
$(\frac{dP}{dT})_c$	2.5×10^6	-2.5×10^6	Pa K^{-1}
	Calculated values		
κ	5.79×10^{-7}	1.11×10^{-6}	m^2 s^{-1}
L	5.996×10^4	-1.04×10^5	J kg^{-1}

We have made a number of simplifying assumptions throughout this paper with regard to the thermal parameters. The first is that we assume a non-zero value of α (e.g. eq. 4), which is incompatible with the assumption of incompressibility. We do not consider the thermal effect on the mechanical equations (i.e. thermal viscoelasticity), and thus the mechanical and thermal parts of the problem interact only at the phase boundaries. This assumption is justified because the temperature perturbation at the boundary owing to the latent heat release is three orders of magnitude larger than that owing to adiabatic compression, which can be deduced by comparing L/c_P with eq. (6). We make the assumption that the conductivity and the diffusivity are the same on both sides of the boundary when applying the boundary conditions and solving the heat equation. The background temperature gradient, dT_o/dr, is assumed to be adiabatic except in the modal result subsection where we will also consider a non-adiabatic gradient for illustrative purposes. Finally, we assume that the kinetics of the phase transitions are unimportant, as discussed in Section 3.

6 RESULTS

In this section we present the results of using phase boundary conditions instead of chemical boundary conditions at the 400 and 670 km discontinuities. The first two subsections examine the direct effects on the modes and the resulting changes in the elastic Love numbers. The next subsection introduces the general effects of phase boundaries. Section 6.4 demonstrates that the displacement fields of internal boundaries clearly show differences between the chemical and phase boundary conditions. However, observations of internal boundary displacements are difficult to obtain and interpret. Finally, we present results for vertical uplift and secular variations of the geoid, which will provide an important constraints in future studies of PGR.

6.1 Modal results

An Earth with phase boundaries has significantly different modal characteristics from an Earth that has only chemical boundaries. Here we extend the conclusions of Johnston *et al.* (1997) regarding the behaviour of the modes in the presence of BD2 conditions in two regards. First, while traditionally ignored at a phase boundary, the buoyancy mode from the density discontinuity does exist but becomes a geostrophic mode (an infinite-period mode of a neutrally stable, inviscid fluid) when the background temperature profile is adiabatic. Secondly, we show that if the background temperature gradient is not adiabatic, then the buoyancy modes no longer have infinite periods.

Johnston *et al.* (1997) introduced an ad hoc parameter ξ into their boundary conditions such that $\xi = 0$ corresponds to BD1 conditions and $\xi = 1$ to BD2 conditions. This parameter also allowed them to consider the removal of latent heat by convective flow through the boundary. They found that the period of the buoyancy mode associated with the phase boundary goes to infinity as $\xi \to 1$ and that the load Love number for horizontal motion, ℓ_l, converges to a non-zero constant.

In the case of BD2 conditions, the infinite-period modes can be interpreted physically. Suppose an entire column of material is displaced upwards adiabatically without changing the pressure at any Eulerian point within the Earth. If the background temperature profile is also adiabatic, the material in the displaced column will have the same temperature as the surrounding material, and so the phase transition will want to occur at the same pressure and depth as in that surrounding material. Assuming the transformation is free to proceed instantaneously, the phase boundary will thus remain fixed at the same Eulerian position in the Earth, and the column of material simply moves through it. There is no displacement of the phase boundary and so no accompanying density anomaly, and hence there is no restoring force on the displaced column. This static displacement is all that would remain of the M1 and M2 modes when the internal boundaries change phase instantaneously and the background temperature distribution is adiabatic. These modes have infinite period, and do not contribute to the radial motion of the density discontinuity. For this reason Mitrovica & Peltier (1989) included the effects of phase boundaries by assuming chemical boundary conditions in all computations, but not including the M1 and M2 modes when summing to obtain displacements in the time domain. However, this method of modelling the phase boundaries does not take into account the changes that occur to the other modes, such as M0, or the contributions of M1 and M2 to horizontal motions through the Love number ℓ_l.

In a neutrally stable, inviscid fluid region of the Earth, such as the outer core, static deformations that do not perturb the density structure (or equivalently the gravitational potential) are called geostrophic modes (Dahlen 1974; Dahlen & Tromp 1998). As described in the preceding paragraph, the static deformation caused by the buoyancy modes of phase boundaries suggests that these modes have become geostrophic modes. Except for the lithosphere, the Earth does behave as though it were a fluid in the $s = 0$ limit (which, for example, is the modal frequency of M1 when there is a phase boundary at 670 km and an adiabatic temperature profile). If the Brunt-Väisälä frequency vanishes in a fluid Earth, as it does in an incompressible homogeneous model, then the Earth is neutrally stable. Hence, there are infinite-period geostrophic modes. For these modes the Earth's density profile cannot change during the motion because that would cause a restoring force and introduce finite modal periods. Thus for geostrophic modes under BD1 conditions, U must vanish at the surface and at internal density discontinuities. In between the boundaries, however, the radial functions must meet the criteria established for geostrophic modes (Dahlen & Tromp 1998): $T_\theta = \Phi = 0$, $T_r = \rho g U$ and $Q = 4\pi G \rho U$. For BD2 conditions, however, it is δR that must vanish at internal boundaries in order to ensure there is no perturbation of the density profile. Because U is discontinuous and no longer associated with the movement of the density discontinuity, it can be non-zero at the boundary. We have confirmed that these criteria, both on the radial functions between the boundaries and on δR at the boundary, are met by M1 as $\xi \to 1$. Therefore, the M1 and M2 modes become geostrophic modes when BD2 conditions are applied and the temperature gradient is adiabatic. The only effect these modes have on any observable quantity is their contribution to horizontal displacements at the outer surface through the Love number ℓ_l. Horizontal surface displacements are possible for geostrophic modes because those displacements do not induce restoring forces. Because geostrophic modes have infinite periods, these horizontal displacements do not exhibit any effects of viscoelastic relaxation, and so they are best viewed as contributing to the Earth's elastic response.

Until now, we have assumed that the background temperature gradient is adiabatic. If this were not the case, then even with BD2 conditions the M1 mode would have a finite period or may even be unstable. To understand this instability, imagine again that a column of material is displaced upwards without changing the Eulerian pressure distribution, but that there is now a superadiabatic background temperature profile. Consider the phase transition at the 400 km boundary that has a positive Clausius–Clapeyron slope. The material in the column is now warmer than the surrounding material, and thus the phase transition in the column occurs at a higher pressure than in the surrounding material. The boundary is therefore displaced downward from where it was before the column was initially uplifted, which causes a buoyancy force that pushes the column up further, which causes the boundary to be depressed further, etc. Thus, this buoyancy mode, M2, is unstable. If one considers the same case applied to the 670 km boundary, where the Clausius–Clapeyron slope is negative, the phase transition occurs at a lower pressure in the upwardly displaced column of material. The boundary is thus displaced upwards from its initial position causing a buoyancy force that pushes the column downward—back to its equilibrium position. In this case, the mode, M1, is stable. One might think that a superadiabatic temperature profile would always produce unstable motions. However, one should remember that we are only considering the stability of the phase transition boundary. The material itself is incompressible and will not interact with the background temperature profile.

In the rest of this paper we assume that the unperturbed temperature gradient and the relationship between pressure and temperature perturbations are always adiabatic. This means that for BD2, the M1 and M2 modes will have infinite periods. When heat conduction is added to the problem, M1 and M2 will have finite periods. In that case, there is a stability argument for these modes similar to that presented above. Because of the assumed adiabatic temperature relationships, the only change in temperature that plays a role in determining the displacements of the phase boundaries is the contribution, θ, from the release of latent heat. Suppose, again, that a column of material at the 400 km discontinuity is displaced upwards, with no accompanying change in the Eulerian pressure distribution. The phase boundary, which was initially carried upward with the column, wants to move back down to its original depth. However, now it cannot do so instantaneously. The reason for this is that as material beneath this elevated boundary begins to change from the high-density phase to the low-density phase, it absorbs heat from the surroundings, thus causing θ to decrease. This decrease in θ causes the phase transformation to want to occur at a lower pressure than before the column was displaced, and so the boundary remains elevated above its original position. The buoyancy force owing to this displaced density discontinuity will cause the column to move back downwards. Therefore, this mode, M2, is stable. A similar argument applied to the 670 km boundary shows that M1 is also stable.

6.2 Elastic load Love numbers

To calculate the elastic load Love numbers, one must consider how the various models of the phase transitions will respond in the

Table 4. Elastic load Love numbers h_l^E and k_l^E for BD1, BD2 and BD4 conditions.

Boundary type/ Boundary thickness	$-h_l^E$			$-k_l^E$		
	2	10	30	2	10	30
BD1	0.4663	0.7296	1.5648	0.2485	0.065 16	0.043 48
BD4/1 km	0.6574	1.0238	1.6573	0.2559	0.075 79	0.045 33
BD4/2 km	0.7858	1.1816	1.6870	0.2610	0.081 39	0.045 92
BD4/5 km	1.0009	1.3936	1.7161	0.2693	0.088 79	0.046 49
BD4/10 km	1.1546	1.5150	1.7292	0.2753	0.092 97	0.046 75
BD2	1.4300	1.6883	1.7447	0.2859	0.098 86	0.047 05

These results are for an incompressible Earth model. Compressibility greatly affects the elastic Love numbers, and the effect of phase boundary conditions would be reduced.

elastic limit. BD2 conditions describe the instantaneous response of a phase boundary to a change in pressure and temperature ignoring the latent heat release. Thus, this boundary condition should change the elastic Love numbers because surface loads can cause instantaneous, elastic changes in the pressure and temperature at depth. For BD3 conditions, all of the latent heat from the transition is released at the boundary. The faster the forcing, the greater the rate of latent heat release. Therefore, for a delta function forcing, all of the latent heat from the transition is released instantly. This heat cannot conduct away from the boundary on short timescales, and the phase transition does not proceed. The elastic Love numbers would thus be the same as for an Earth with a chemical boundary. This result can be understood in the Laplace transform domain by noting that the temperature perturbation becomes infinite in eq. (17) as $s \to \infty$, which eventually causes the boundary condition, eq. (20), to reduce to $U_+ = U_-$ (let $\theta_{lo} \to \infty$ in eq. 20). This argument does not hold for BD4 conditions, however. The latent heat is still released instantly, but the source of that latent heat is now distributed over a boundary region with non-zero thickness. If one looks at the temperature perturbation at a particular point, that point can see the heat released by phase changes occurring at its own position plus the heat released in some volume dV around it. As s increases (i.e. at shorter time intervals after the load is applied), the local concentration of heat that was released at the point increases, but the volume that the point can see around it decreases. This has the net effect of causing the temperature perturbation at that point to be finite as $s \to \infty$. Thus, even at the shortest timescales, the boundary conditions do not reduce to those of BD1, and so BD4 and BD1 elastic Love numbers are different.

Generally, finding the elastic load Love numbers from the techniques described earlier is simple: one replaces the s-dependent functions $\lambda(s)$ and $\mu(s)$ with their elastic values λ and μ and finds h_l and k_l in the usual way. However, it is more difficult for the BD4 conditions. The latent heat enters into the problem explicitly, and one must solve the problem in the Laplace domain. We take θ_{lo} at $s = 10^{-6}$ s^{-1} to be the $s \to \infty$ limit and assume that the solution for this value of s is the elastic response. We settled on this value of s after repeating these calculations for a number of other large-s values and noting that the temperature perturbation in the Laplace domain had converged when s was as large as 10^{-6} s^{-1}. Table 4 shows the values of h_l^E for four different boundary thicknesses for the BD4 conditions as well as the solutions for the BD1 and BD2 conditions. Note that the difference can be as large as a factor of 3 for $l = 2$. Phase boundary conditions do not affect k_l^E to the same extent as h_l^E, but can still be significant. For example, k_{10}^E for BD2 conditions differs by 50 per cent from k_{10}^E for BD1 conditions.

The predictions for the elastic body Love numbers also vary depending upon boundary type, but not to the extent of the load Love numbers. Table 5 shows the variations in the predictions of h_2^B and k_2^B where the superscript B represents the body Love numbers. Note that k_2^B, used in calculations of the luni-solar body tides and the Chandler wobble, only has a 3 per cent difference between the BD1 and BD2 conditions. However, a change of this size can have a significant impact on estimates of the Chandler wobble period (Smith & Dahlen 1981).

This difference in the elastic Love numbers suggests the interesting prospect of trying to find discrepancies between the observed elastic response of the Earth to applied loads, such as that from ocean tidal loading (e.g. Melchior & Francis 1996), and the predictions from traditional calculations based upon the load Love numbers for BD1 conditions. However, there are two factors to consider when interpreting these results. First, compressibility makes a large difference in the Love numbers. Using a code that calculates Love numbers for an elastic Earth represented by PREM, we find the difference between the two extreme conditions (BD1 and BD2) reduces to 32 per cent for h_2^E and 1 per cent for k_2^B (Tamisiea & Wahr 2002). Secondly, we have not considered kinetics, which might be the dominant mechanism preventing a change of phase for the relatively small motions caused by ocean tidal loading and the Chandler wobble, as was discussed in Section 3.

6.3 General effects of conductivity

In the following subsections, we will show results computed using the four different boundary types. (Note that all of the following results are found by summing the solutions for spherical harmonic degrees 2–30.) As a typical example, consider Fig. 5, which presents results for the present-day maximum displacement of the 670 km boundary under Canada. Results such as those shown in this figure will be interpreted in the following subsection. To generate these

Table 5. Elastic body Love numbers h_l^B and k_l^B for BD1, BD2 and BD4 conditions.

Boundary type/ Boundary thickness	h_2^B	k_2^B
BD1	0.5551	0.3066
BD4/1 km	0.6007	0.3084
BD4/2 km	0.6324	0.3097
BD4/5 km	0.6870	0.3119
BD4/10 km	0.7272	0.3136
BD2	0.8001	0.3165

These results are for an incompressible Earth model. Compressibility greatly affects the elastic Love numbers, and the effect of phase boundary conditions would be reduced.

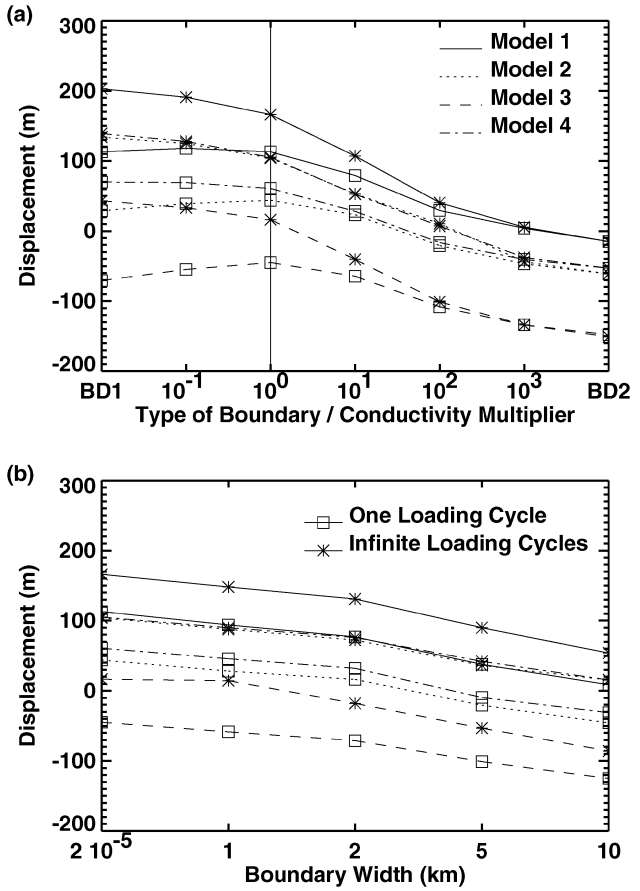

Figure 5. Maximum displacement of the 670 km boundary for: (a) BD1 and BD2 conditions (shown at the left- and right-hand edges of the plot), and for BD3 conditions with various values of conductivity and (b) BD4 conditions. In (a), the numbers indicate the factor that multiplies the conductivities given in Table 3. The solid vertical line indicates the results obtained with the assumed conductivity values given in Table 3. In (b), the conductivities are always taken to be the assumed values shown in Table 3. The viscosity models are given in Table 2.

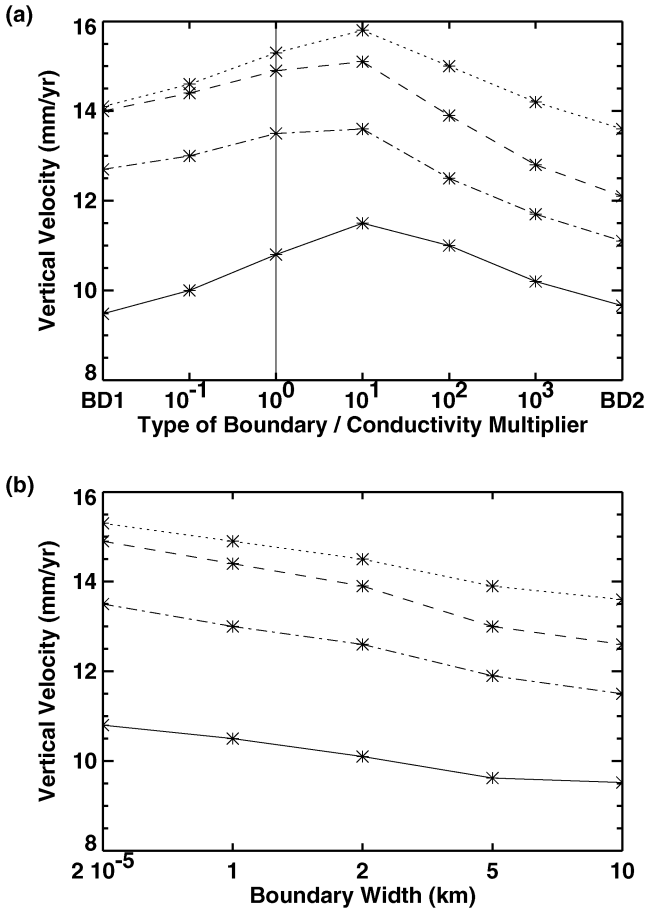

Figure 6. Maximum vertical velocity at the surface for: (a) BD1 and BD2 conditions, and for BD3 conditions with various values of conductivity and (b) BD4 conditions. The symbols and line styles are defined in Fig. 5.

results, we used the ICE-3G deglaciation history as an applied surface load, assuming either one loading cycle or an infinite number of them. We then computed the Earth's response to this load for the four boundary types, assuming different viscosity models, different conductivity values (for BD3 conditions) and different boundary thicknesses (for BD4 conditions). We extracted the present-day displacement field from the results in each case, and searched for the largest value of that displacement field. The results are plotted in this figure. The top plot shows results for BD1 and BD2 conditions, as well as for BD3 conditions with various values of thermal conductivity. As we described previously, one would expect that low values of conductivity would return BD1-type results and high values would return BD2-type results. The numbers on the x-axis of these graphs indicate the multiplicative factor of the conductivities in Table 3. The solid vertical line represents the results for the assumed values listed in Table 3. The factors of ten on either side of this line are included to determine the effect that underestimating or overestimating the conductivity would have on the final results. The factors of 10^2 and 10^3 are included to illustrate the smooth transition to the BD2 limit.

For all quantities, one observes a fairly smooth transition between the two extreme limits (BD1 and BD2 conditions). However, this trend is not always monotonic. On some occasions, the signal exhibits a maximum or minimum between the limits. An example of this is shown in Fig. 5(a) for BD3 conditions, viscosity Model 3, and one loading cycle. The reason for this is not clear. The periods of the M1 and M2 modes are probably growing longer as the conductivity increases, and perhaps the individual responses at each wavelength conspire to give a larger response. Occasionally, as in the case of the surface uplift velocity (Fig. 6) for Model 1 and one loading cycle, the maximum amplitude of the BD2 response is larger than the amplitude of the BD1 response. For this Earth model, the contribution from M1 to the surface radial velocity for BD1 conditions is positive. Thus, if one naively removed M1, the signal would decrease, not increase as is observed. We also examined the M0 and L0 modes and found that their individual contributions to the signal both increased in the case of BD2 conditions as compared with BD1 conditions.

Maximum displacement values, such as those shown in Fig. 5, are always found in a region underlying the position of the Laurentide ice sheet, with latitudes of between 20°N and 70°N and longitudes of between 10°W and 150°W. There may be values that are larger in other parts of the globe, especially over Antarctica. However, the PGR component of surface signals is easier to identify over Canada, whereas the current ice mass changes affect the signals over Antarctica.

The results shown in Fig. 5, which are typical for most observables, suggest that for most of the viscosity models, the number of

loading cycles has almost no effect on the results for BD2 conditions. Because the long-term contributions from M1 and M2 have disappeared from the viscous response, a single loading cycle does not excite any modes of period longer than the loading cycle. The only arguable exception occurs for Model 3 which has the largest viscosity discontinuity, and it is still nearly true even in that case.

The lower panel in Fig. 5 shows results for BD4 conditions with various boundary thicknesses. The results for the 2 cm boundary shown at the left-hand edge of the panel agree well with the results for the BD3 boundary condition in the top panel. Note that in order for the thickness of the boundary to have much effect on the results, the boundary must be thicker than 1 km. The 10 km boundary generally gives results that are consistent with an increase of conductivity in the narrow boundary case (BD3) by one to two orders of magnitude. The results generally decrease monotonically with increasing boundary thickness.

6.4 Internal boundary displacements

Because the modes associated with a boundary have the largest effect on that boundary, it is not surprising that the displacements of the internal boundaries show the greatest change with the introduction of the phase boundary conditions. Thus, observations of the position of the boundaries could put an additional constraint on the PGR model if one could isolate the contribution from the rebound alone. As an example, Fig. 7 shows the topography of the 670 km boundary

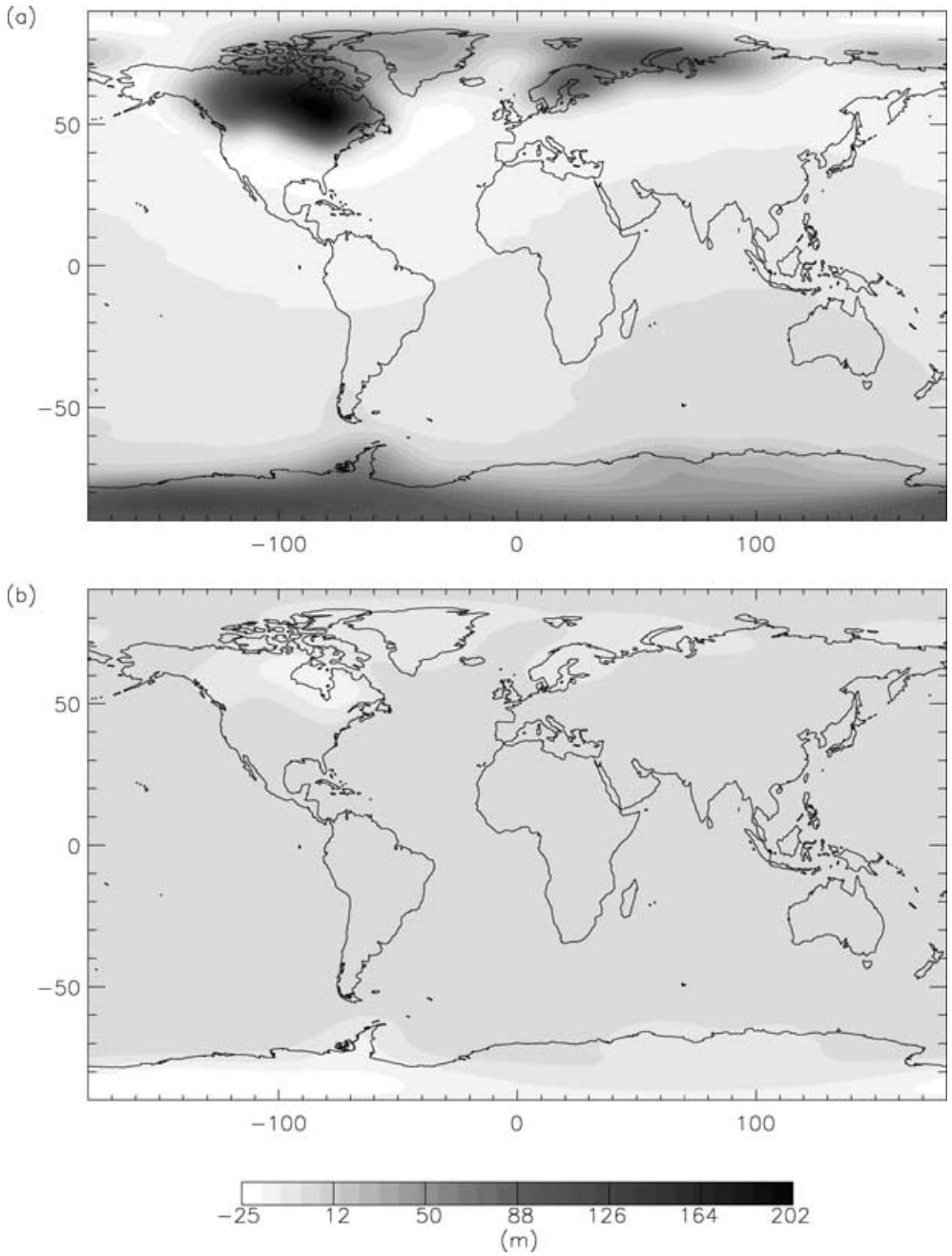

Figure 7. Topography of the 670 km boundary for (a) BD1 and (b) BD2 conditions after an infinite number of loading cycles for Model 1. Note the opposite direction of the displacement for the two types of boundary conditions.

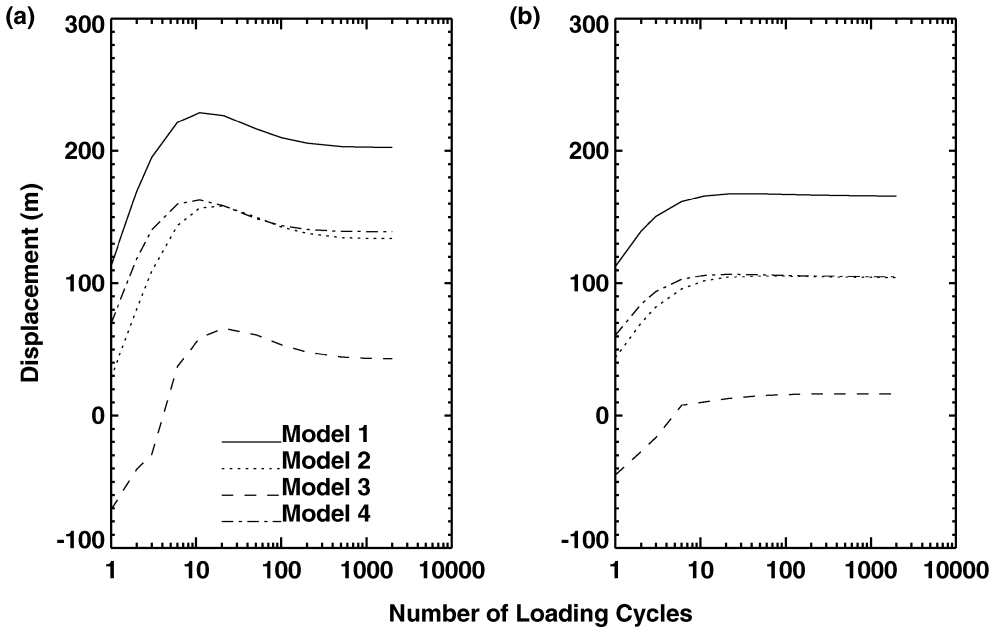

Figure 8. Maximum displacement of the 670 km boundary as a function of the number of loading cycles for: (a) BD1, and (b) BD3 conditions with the thermal conductivities listed in Table 3. Note that the displacement of the boundary varies less as a function of loading cycles for BD3 conditions than it does for BD1 conditions.

calculated for an infinite number of loading cycles and Model 1. The maximum uplift for BD1 conditions is 200 m, while the boundary is displaced downward 15 m for BD2 conditions. Hence, in theory if one knew the current position of the boundary, one would be able distinguish between the different types of boundaries. Many other factors, however, enter into the solution and make the interpretation of boundary position difficult.

The number of loading cycles used (if two or greater) generally only has a small effect on surface observations (e.g. Johnston & Lambeck 1999). The effect on displacement of the internal boundaries, however, is much larger. Fig. 8 shows a plot of the maximum displacement of the 670 km boundary under the Laurentide ice sheet versus the number of loading cycles for the four viscosity models. The maximum displacement for BD1 conditions occurs after 10–20 loading cycles and only decreases by around 20 per cent from there. This decrease is a result of the long-term loading effect of the 400 km boundary on the 670 km boundary. The mode M2 has both a longer period and the opposite contribution to displacement at 670 km compared to M1, which explains the shape of the curve in Fig. 8(a). When conductivity is introduced into the problem, the boundary effectively comes to equilibrium after a much smaller number of loading cycles. A closer inspection of the results indicate that the maximum occurs later, as one would expect if the period of M2 were becoming longer. It is also likely, although impossible to check because of our use of the collocation technique, that the contribution of M2 to the displacement of 670 km decreases. One can imagine that as the phase transitions become more important causing the periods of M1 and M2 to become longer, other modes with much shorter periods such as M0, L0 and C0 govern the motion of the density discontinuities.

As mentioned earlier, Fig. 5 shows the maximum radial displacement of the 670 km boundary for the four different boundary conditions and different values of conductivity. By comparing the results for Models 2 and 4, one can see that the displacement at 670 km after an infinite number of loading cycles is insensitive to the upper-mantle viscosity profile. However, the displacement of the 400 km boundary is much more dependent on the upper-mantle viscosity, as one would expect. The chemical boundary results agree qualitatively with those found by Wu (1990). Nevertheless, the amplitudes presented here are smaller because Wu used a single-disc ice sheet, which has a greater mass per unit area at the surface than the ICE-3G model we use.

As with all predictions of observables, uncertainties in the viscosity profile have a large effect on the answers. However, if one were able to use observations to identify the PGR portion of the topography on an internal boundary, and those observations were used to infer viscosity without accounting for the phase transitions at the 400 and 670 km boundaries, one could make a error in the inferred viscosity. After an infinite number of loading cycles, for example, the displacement of a 5 km thick boundary at 670 km for Model 2 is nearly the same as the displacement for BD1 conditions of Model 3, which has a viscosity that is a factor of 4 larger.

However, the practical use of these estimates is difficult. Seismic observations show that the boundaries have large topographies, ± 15 km, on both large scales (Flanagan & Shearer 1998, 1999) and short scales (Dueker & Sheehan 1998). This topography is much larger than that predicted from PGR and is presumably a result of convective processes. If the error in the seismic estimates were small, one could try to fit the general PGR pattern to this topography. However, the observational errors are generally of the order of the thickness of the boundary or larger. Thus, displacements as small as 100 m would be impossible to detect.

6.5 Surface observations

There are many surface observations that are used as constraints in PGR modelling. Many of these signals, however, can have large contributions from other geophysical processes. In this final subsection, we illustrate the possible effects of phase boundaries on three surface observations: vertical uplift, $\dot{J}_l$, and the secular change of the geoid. We have chosen these because new space geodetic techniques, such as GPS and GRACE, will give us new constraints in

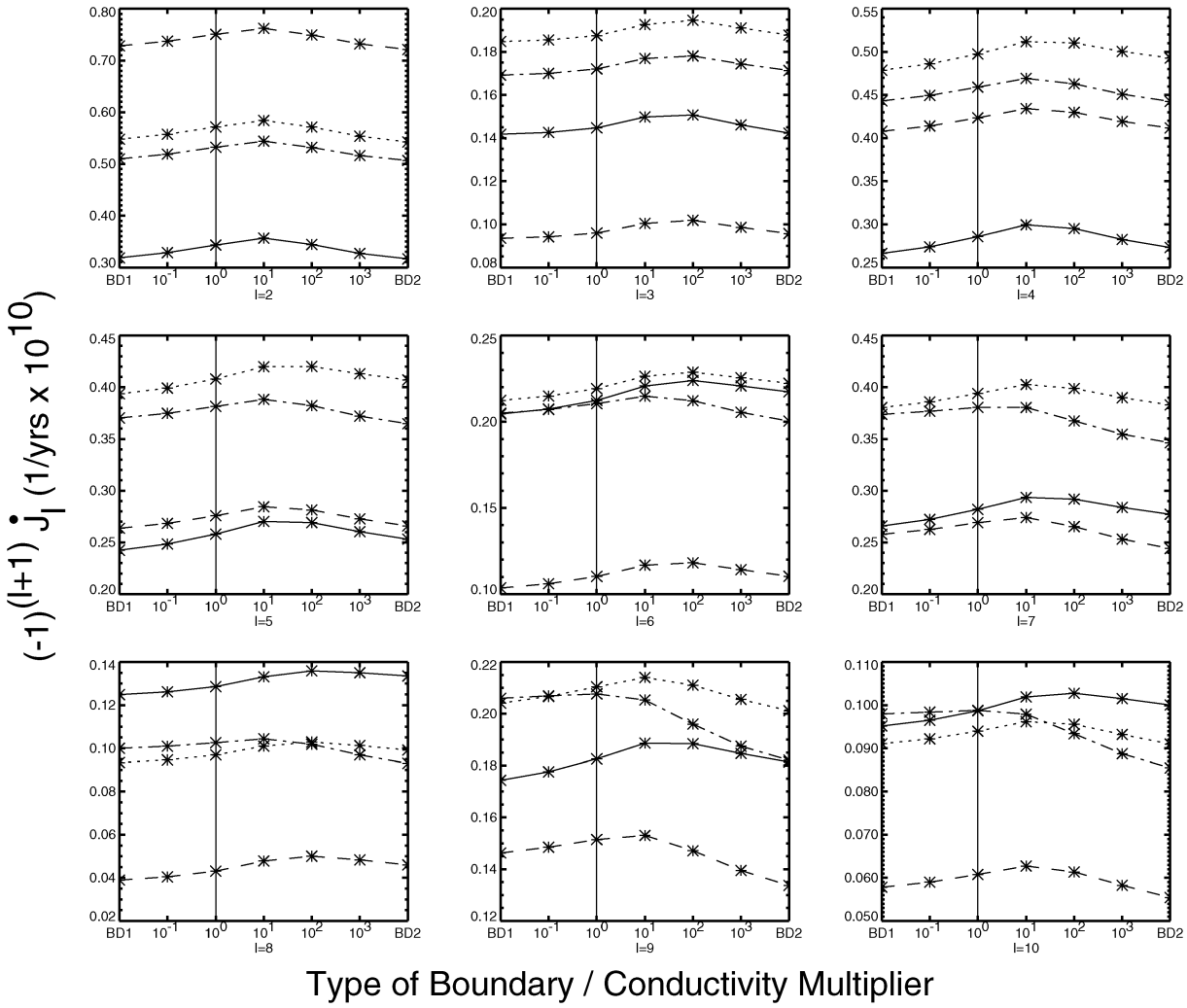

Figure 9. Values of $\dot{J}_l$ for BD1 and BD2 conditions, and for BD3 conditions with various values of conductivity. The symbols and line styles are defined in Fig. 5.

the years to come. We also list the results for several other commonly investigated surface observations. As one would expect, the long-period modes contribute little to rate of change observations, and thus these observations are insensitive to the number of loading cycles. Therefore, the graphs in this section will only present results for an infinite number of loading cycles.

Both vertical and horizontal motion give constraints on PGR models. Each of these has drawbacks, however. Horizontal motion is much more sensitive to the ice sheet parametrization, lateral variations in viscosity and lithospheric thickness than is vertical motion (e.g. Mitrovica *et al.* 1994). Yet vertical rates derived from GPS measurements have larger errors than horizontal rates. GPS vertical motions reliable to 1 mm yr^{-1}, which is the level of accuracy needed to differentiate between different models of viscosity, require about 5 yr or more of continuous measurements (Larson & van Dam 2000). One of the best examples of GPS data for use in PGR is the BIFROST campaign in the Fennoscandian region (Scherneck *et al.* 1998; Milne *et al.* 2001). Fig. 6 shows the radial velocity predicted at the surface for various models. For BD1 conditions, one can note that a viscosity jump of 5 or 20 at 670 km gives roughly the same result. This is a commonly known, general feature of all rate of change surface observables we have considered; i.e. that the same results can be obtained from both a small and a large jump in the viscosity. For radial velocities the BD3 conditions cause a 6–15 per cent variation in the results, whereas a 2 km wide boundary causes a 1–7 per cent variation from the BD1 solutions.

Three dedicated gravity missions have recently been approved: CHAMP, GRACE and GOCE. In particular, GRACE (Gravity Recovery and Climate Experiment) will have the accuracy needed to detect the time-varying portion of the gravity field up to degree and order of 70, and is similar to the SST mission described in Dickey *et al.* (1997). Currently, the most common space-based measurement of the PGR contribution to time-variable gravity are satellite laser-ranging measurements of secular variations of the zonal harmonics, $\dot{J}_l$. These are the scaled, $m = 0$ coefficients in the spherical harmonic expansion of the secular change in the geoid height (e.g. Chao & Gross 1987). Fig. 9 shows the variation of the zonal harmonics for BD1, BD2 and BD3 boundary conditions, and Fig. 10 shows the variation for BD4 conditions. Note that the $(-1)^{l+1}$ factor has been included so that all of the coefficients are displayed as positive. Data from LAGEOS and Starlette have been used to obtain the time-varying portion of the lowest-degree even harmonics, but there is difficulty in obtaining the odd-degree solution (e.g. Yoder *et al.* 1983; Rubincam 1984).

Many other processes can contribute to $\dot{J}_l$, including ongoing changes in the ice masses over Greenland and Antarctica. It is

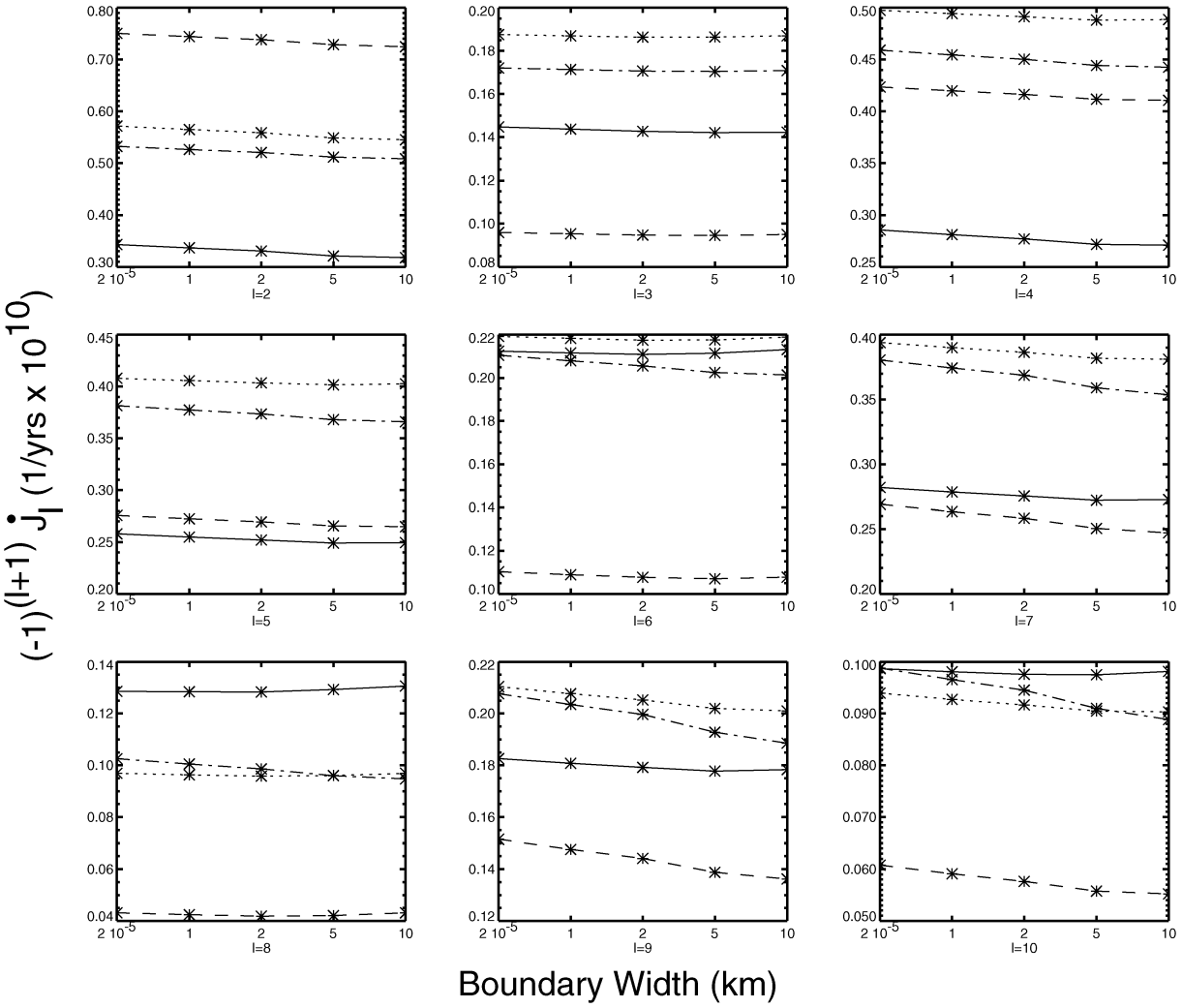

Figure 10. Values of $\dot{J}_l$ for BD4 conditions with various boundary widths. The symbols and line styles are defined in Fig. 5.

possible to eliminate the signal from Antarctica if one had the odd degrees (James & Ivins 1997), but the signal from Greenland would still contaminate the result. One will probably have to look at the signal regionally instead of globally to remove all of the other 'noise' signals. This is where the shorter wavelengths available with GRACE offers an improvement over previous satellite gravity missions (see, for example, Wahr & Davis 2002). The maximum secular geoid change is shown in Fig. 11.

A BD3 boundary would cause a 3–9 per cent error in the secular variation of the geoid for a particular viscosity profile if BD1 conditions are used to model the rebound. If one assumes BD4 boundary conditions, the situation becomes better and the variation from the BD1 solutions is reduced to 3 per cent or less. It is unclear, however, how well the viscosity profile itself can be determined using this type of data. Initial tests show that the ice sheet parametrization will play a large role in the final signal. One would need to perform a joint inversion for both the ice sheet parametrization and the viscosity profile to determine how well this information can be inferred.

Finally, Table 6 summarizes the likely range of phase boundary effects for a wide variety of observations. The results provide a general idea of the level at which the phase boundary conditions become important for particular measurements. As mentioned in Section 6.3, the perturbation from the BD1 solutions are not necessarily monotonic as one increases either the thermal conductivity or the boundary width. For example, BD3 conditions increase the signal of observables that do not depend upon the number of loading cycles, such as the rate of change measurements, while BD2 conditions generally decrease the same signals from the BD1 predications. Table 6 also lists the perturbations of relative sea level (RSL), which has been a prominent measurement in past studies. Mitrovica & Peltier (1993) found that near the centres of ice sheets, the RSL curves can be modelled as $A(\mathrm{e}^{-t/\tau} - 1)$ and that τ is sensitive to the viscosity profile. For this example, we calculated the values of $1/\tau$ from predictions of RSL curves at Hudson Bay. The largest perturbations from the BD1 solutions (63 per cent for BD2 conditions and 31 per cent for BD4 conditions) occur for Model 3, which has the largest viscosity jump at 670 km. In these two cases, the phase transitions effectively allow the Earth to relax on shorter timescales and would cause one to underestimate the value of lower-mantle viscosity if observations were compared with predictions calculated using BD1 conditions (Johnston *et al.* 1997). A general conclusion from the results in this table is that any attempt to improve a viscosity model by trying to match observational discrepancies that are of the order of the 5–10 per cent level may be limited by our imperfect knowledge of the characteristics of the internal boundaries.

Table 6. Summary of percentage perturbations from BD1 solutions for BD2, BD3, and BD4 conditions.

Observation	Loading cycles	per cent perturbation		
		BD2	BD3	BD4
670 km displacement	1	−312 to 109	−37 to 52	−172 to 43
	∞	−451 to −107	−62 to −18	−224 to −56
400 km displacement	1	−291 to 80	−212 to 453	−175 to 15
	∞	−422 to −113	−44 to −15	−256 to −66
Surface displacement	1	−39 to −19	5 to 19	−21 to −9
	∞	−64 to −34	−10 to −6	−38 to −19
Uplift velocity	1	−13 to 4	6 to 15	−8 to 1
	∞	−13 to 2	6 to 15	−8 to 2
Geoid anomaly	1	−28 to −9	1 to 15	−14 to −5
	∞	−55 to −15	−8 to −2	−30 to −8
Rate of change of geoid	1	−7 to 1	3 to 9	−3 to 2
	∞	−7 to 0	3 to 9	−3 to 1
Free air gravity anomaly	1	−22 to −13	−1 to 5	−13 to −6
	∞	−39 to −16	−7 to −3	−22 to −9
$\dot{J}_2$	1	−1 to 0	3 to 7	0 to 1
	∞	−2 to −1	3 to 8	0 to 1
$1/\tau$ (RSL)	1	6 to 62	−10 to 3	2 to 30
	∞	8 to 63	−10 to 3	3 to 31

For the BD4 conditions, these results are for a 5 km thick boundary. The range in perturbations listed is a result of variations in the results for different viscosity profiles. If x is the percentage perturbation, then the solution for a given quantity can be found by multiplying $(1 + x/100)$ times the BD1 value.

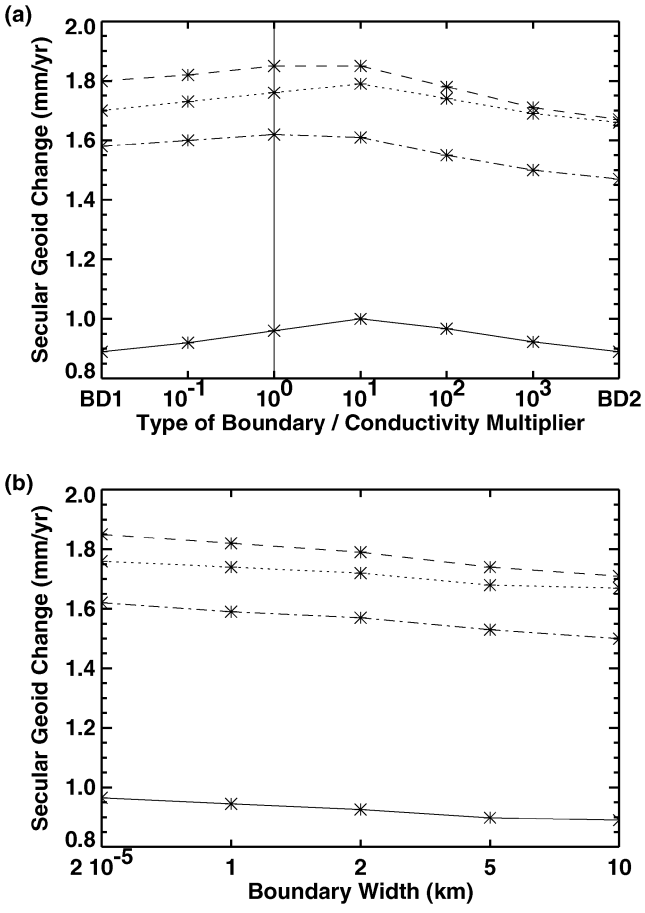

Figure 11. Maximum secular change of the geoid height for: (a) BD1 and BD2 conditions, and for BD3 conditions with various values of conductivity and (b) BD4 conditions. The symbols and line styles are defined in Fig. 5.

7 CONCLUSIONS

Our objective is to better understand the possible effects of mantle phase transitions on PGR. The results are relevant to the interpretation of PGR observations for at least two reasons. One is that they may indicate whether or not those observations could be used to learn more concerning the characteristics of the 400 and 670 km discontinuities. The other reason is that studies that have used PGR observations to learn about the Earth's viscosity have, with only a few exceptions, ignored the effects of phase transitions. The results described in this paper are thus useful for estimating the errors that could be introduced into those viscosity solutions if the internal boundaries behave as phase boundaries but are incorrectly modelled as chemical boundaries.

Modelling the effects of phase transitions is complicated by two factors: the release of latent heat during the phase transformation and the presence of a potential energy barrier related to the kinetics of the phase change. In the models described above we have included the release of latent heat, but not the kinetics. These models extend earlier models by including the effects of latent heat through the heat conduction equation. The importance of those effects depends on the thermal conductivity of the material near the boundary and on the thickness of the boundary region, neither of which are well known for either the 400 or 670 km boundary. The boundary thickness is especially uncertain.

Phase transitions at an internal boundary are particularly important because of their effect on the buoyancy mode associated with particle displacements at that boundary. In previous studies it has usually been assumed that a buoyancy mode has no impact on the PGR solution when the boundary is a phase boundary. We have found that this is correct only if the material surrounding the boundary is stratified adiabatically and if there is no release of latent heat during the phase transformation (or, equivalently, if the thermal conductivity is infinite). In that case, the buoyancy mode reduces to an infinite-period geostrophic mode. Yet if the background temperature

is not adiabatic then the buoyancy mode can have a finite period or even be unstable. If the temperature distribution is adiabatic and the effects of latent heat are included, the buoyancy mode will be stable but will have a finite period. In fact, the most important consequence of latent heat release in terms of its impact on the PGR solution is that it causes buoyancy modes to make non-negligible contributions to the deformation.

The numerical results presented in Section 6 show that if the internal boundaries at 400 and 670 km are phase boundaries but are incorrectly modelled as chemical boundaries, there will be 5–10 per cent errors in the model predictions of the most useful PGR observables, including geoid and gravity anomalies, the secular change in the geoid, relative sea level changes and the radial motion of the outer surface. These estimates of the errors introduced by incorrectly modelling the boundaries should be interpreted as upper limits; the large density jumps at the boundaries in our rheology model may cause the importance of the boundaries to be overestimated. Overall, though, these results suggest that there is not much point in trying to refine a viscosity or ice deglaciation model to explain a 5–10 per cent disagreement with a PGR observation unless the phase boundary effects are well understood.

The one component of PGR on which phase transformations can have a dramatic effect is the topography of internal boundaries. The effects of phase transformations on that topography are typically of the same order as the uncertainty caused by imperfect knowledge of the viscosity profile. It is unlikely, though, that observations of internal boundary topography could be used to learn more concerning the characteristics of these phase transformations. The topography caused by PGR is predicted to be of the order of a few hundred metres, at most. Seismic observations, on the other hand, suggest that the total topography on those boundaries is of the order of ± 15 km. These large topographic amplitudes are presumably the result of convective flow unrelated to PGR, and cannot be predicted independently to anywhere near the accuracy required to determine the PGR contributions. In fact, our tentative conclusion is that there is little hope of using any PGR observations in the near future to learn about phase transitions at internal boundaries.

One intriguing conclusion, though, from Section 6.2 is that the elastic Love numbers could be modified significantly by the presence of phase transformations at the 400 and 670 km boundaries, if the width of the phase transition zone is a kilometre or more. This suggests that observations of the luni-solar body tide, the ocean load tide, or the Chandler Wobble period (which depends on the elastic $l = 2$ body tide Love number; see Smith & Dahlen 1981) might provide useful information concerning the characteristics of the phase transitions. However, this conclusion does not consider the effects of kinetics, which could severely hinder the phase transformations for the small displacements and relatively short timescales associated with these motions. Nevertheless, we believe that these results warrant a closer examination of the kinetic processes responsible for phase transitions in the case of these near-equilibrium, small-amplitude motions.

ACKNOWLEDGMENTS

We would like to thank Pamela Burnley for conversations regarding kinetics and Richard O'Connell for suggesting inclusion of thick boundaries into the theory. In addition, we thank Detlef Wolf and two anonymous referees for their insightful reviews. This work was supported by NSF Grant no EAR-9526905 to the University of Colorado and a CIRES Graduate Fellowship (MET).

REFERENCES

Anderson, D.L., 1989. *Theory of the Earth,* Blackwell, London.

Bina, C.R. & Helffrich, G., 1994. Phase transition Clapeyron slopes and transition zone seismic discontinuity topography, *J. geophys. Res.,* **99,** 15 853–15 860.

Buffett, B.A., 1993. Evolution of a phase change boundary in a time varying pressure field, *EOS, Trans. Am. geophys. Un.,* **74,**, Suppl., 52.

Chao, B.F. & Gross, R.S., 1987. Changes in the Earth's rotation and low-degree gravitational field induced by earthquakes, *Geophys. J. R. astr. Soc.,* **91,** 569–596.

Christensen, U.R., 1985. Mantle phase transitions and postglacial rebound, *J. geophys. Res.,* **90,** 11 312–11 318,

Christensen, U.R. & Yuen, D.A., 1985. Layered convection induced by phase transitions, *J. geophys. Res.,* **90,** 10 291–10 300.

Däßler, R. & Yuen, D.A., 1996. The metastable olivine wedge in fast subduction slabs: constraints from thermo-kinetic coupling, *Earth planet. Sci. Lett.,* **137,** 103–118.

Dahlen, F.A., 1974. On the static deformation of an Earth model, *Geophys. J. R. astr. Soc.,* **36,** 461–485.

Dahlen, F.A. & Tromp, J., 1998. *Theoretical Global Seismology,* Princeton University Press, Princeton, NJ.

Defraigne, P., Dehant, V. & Wahr, J.M., 1996. Internal loading of an inhomogeneous compressible earth with phase boundaries, *Geophys. J. Int.,* **125,** 173–192.

Dehant, V. & Wahr, J.M., 1991. The response of a compressible, non-homogeneous Earth to internal loading: theory, *J. Geomag. Geoelectr.,* **43,** 157–178.

Devaux, J.P., Schubert, G. & Anderson, C., 1997. Formation of a metastable olivine wedge in a descending slab, *J. geophys. Res.,* **102,** 24 627–24 637.

Dickey, J.O. *et al.*, 1997. *Satellite Gravity and the Geosphere,* National Academy Press, Washington, DC.

Dueker, K.G. & Sheehan, A.F., 1998. Mantle discontinuity structure beneath the Colorado Rocky Mountains and High Plains, *J. geophys. Res.,* **103,** 7153–7169.

Dziewonski, A.M. & Anderson, D.L., 1981. Preliminary reference Earth model, *Phys. Earth planet. Inter.,* **25,** 297–356.

Flanagan, M.P. & Shearer, P.M., 1998. Global mapping of topography on transition zone velocity discontinuities by stacking *SS* precursors, *J. geophys. Res.,* **103,** 2673–2692.

Flanagan, M.P. & Shearer, P.M., 1999. A map of topography on the 410-km discontinuity from *PP* precursors, *Geophys. Res. Lett.,* **26,** 549–552.

Gasparik, T., 1990. Phase relations in the transition zone, *J. geophys. Res.,* **95,** 15 751–15 769.

Gasparik, T., 1993. The role of volatiles in the transition zone, *J. geophys. Res.,* **98,** 4287–4299.

Gjevik, B., 1972. Surface readjustment owing to a subcrustal phase transition, *Phys. Earth planet. Inter.,* **5,** 403–408.

Han, D., 1993. *A New Analysis of Post Glacial Rebound and an Analysis of Anisotropy of the Mantle Rheology, PhD thesis,* University of Colorado, Boulder, CO.

Hanyk, L., Matyska, C. & Yuen, D.A., 1998. Initial-value approach for viscoelastic responses of the Earth's mantle, in *Dynamics of the Ice Age Earth: a Modern Prospective,* pp. 135–154, ed. Wu, P., Trans Tech Publications, Ltd.

Hofmeister, A.M., 1999. Mantle values of thermal conductivity and the geotherm from phonon lifetimes, *Science,* **283,** 1699–1706.

Ito, E. & Katsura, T., 1989. A temperature profile of the mantle transition zone, *Geophys. Res. Lett.,* **16,** 425–428.

Jackson, I. & Rigden, S.M., 1998. Composition and temperature of the Earth's mantle: seismological models interpreted through experimental studies of earth materials, in *The Earth's Mantle: Composition, Structure, and Evolution,* pp. 405–460, ed. Jackson, I., Cambridge University Press, Cambridge.

James, T.S. & Ivins, E.R., 1997. Global geodetic signatures of the Antarctic ice sheet, *J. geophys. Res.,* **102,** 605–633.

Jeanloz, R. & Thompson, A.B., 1983. Phase transitions and mantle discontinuities, *Rev. Geophys. Space Phys.,* **21,** 51–74.

Johnston, P. & Lambeck, K., 1999. Postglacial rebound and sea level contributions to changes in the geoid and the Earth's rotation axis, *Geophys. J. Int.,* **136,** 537–558.

Johnston, P., Lambeck, K. & Wolf, D., 1997. Material versus isobaric internal boundaries in the Earth and their influence on postglacial rebound, *Geophys. J. Int.,* **129,** 252–268.

Kerschhofer, L., Dupas, C., Liu, M., Sharp, T.G., Durham, W.B. & Rubie, D.C., 1998. Polymorphic transformations between olivine, wadsleyite and ringwoodite: mechanism of intracrystalline nucleation and the role of elastic strain, *Mineral. Mag.,* **62,** 617–638.

Kirby, S.H., Stein, S., Okal, E.A. & Rubie, D.C., 1996. Metastable mantle phase transformations and deep earthquakes in subduction oceanic lithosphere, *Rev. Geophys.,* **34,** 261–306.

Larson, K.M. & van Dam, T., 2000. Measuring postglacial rebound with GPS and absolute gravity, *Geophys. Res. Lett.,* **27,** 3925–3928.

Melchior, P.J. & Francis, O., 1996. Comparison of recent ocean tide models using groundbased tidal gravity measurements, *Mar. Geol.,* **19,** 291–330.

Milne, G.A., Davis, J.L., Mitrovica, J.X., Scherneck, H.-G., Johansson, J.M., Vermeer, M. & Koivula, H., 2001. Space-geodetic constraints on glacial isostatic adjustment in Fennoscandia, *Science,* **291,** 2381–2385.

Mitrovica, J.X. & Peltier, W.R., 1989. Pleistocene deglaciation and global gravity field, *J. geophys. Res.,* **94,** 13 651–13 671.

Mitrovica, J.X. & Peltier, W.R., 1992. A comparison of methods for the inversion of viscoelastic relaxation spectra, *Geophys. J. Int.,* **108,** 410–414.

Mitrovica, J.X. & Peltier, W.R., 1993. A new formalism for inferring mantle viscosity based on estimates of post glacial decay times: application to RSL variations in N.E. Hudson Bay, *Geophys. Res. Lett.,* **20,** 2183–2186.

Mitrovica, J.X., Davis, J.L. & Shapiro, I.I., 1994. A spectral formalism for computing three-dimensional deformations due to surface loads: 2. Present-day glacial isostatic adjustment, *J. geophys. Res.,* **99,** 7075–7101.

Nakada, M. & Lambeck, K., 1989. Late Pleistocene and Holocene sea-level change in the Australian region and mantle rheology, *Geophys. J. R. astr. Soc.,* **96,** 497–517.

O'Connell, R.J., 1976. The effects of mantle phase changes on postglacial rebound, *J. geophys. Res.,* **81**.

Özişik, M.N., 1993. *Heat Conduction,* 2nd edn, Wiley, New York.

Peltier, W.R., 1974. The impulse response of a Maxwell Earth, *Rev. Geophys. Space Phys.,* **12,** 649–669.

Rubie, D.C., 1993. Mechanisms and kinetics of reconstructive phase transformations in the Earth's mantle, in *Experiments at High Pressure and Applications to the Earth's Mantle: Mineralogical Association of Canada Short Course Handbook,* pp. 274–303, ed. Luth, R.W. Mineralogical Association of Canada, Nepean, ON.

Rubie, D.C. & Ross, C.R., 1994. Kinetics of the olivine–spinel transformation in subducting lithosphere: experimental constraints and implications for deep slab processes, *Phys. Earth planet. Inter.,* **86,** 223–241.

Rubincam, D.P., 1984. Postglacial rebound observed by Lageos and the effective viscosity of the lower mantle, *J. geophys. Res.,* **89,** 1077–1088.

Saxena, S.K., 1996. Earth mineralogical model: Gibbs free energy minimization computation in the system MgO-FeO-SiO_2, *Geochim. Cosmochim. Acta,* **60,** 2379–2395.

Scherneck, H.G., Johansson, J.M., Mitrovica, J.X. & Davis, J.L., 1998. The BIFROST project: GPS determined 3-D displacement rates in Fennoscandia from 800 days of continuous observations in the SWEPOS network, *Tectonophysics,* **294,** 305–321.

Schubert, G., Yuen, D.A. & Turcotte, D.L., 1975. Role of phase transitions in a dynamic mantle, *Geophys. J. R. astr. Soc.,* **42,** 705–735.

Smith, M.L. & Dahlen, F.A., 1981. The period and Q of the Chandler Wobble, *Geophys. J. R. astr. Soc.,* **64,** 223–282.

Solomatov, V.S. & Stevenson, D.J., 1994. Can sharp seismic discontinuities be cause by non-equilibrium phase transformations, *Earth planet. Sci. Lett.,* **125,** 267–279.

Tamisiea, M.E. & Wahr, J.M., 2002. Phase transitions and short timescale sinusoidal motions, *Earth planet. Sci. Lett.,* in press.

Tushingham, A.M. & Peltier, W.R., 1991. ICE-3G: a new global model of late Pleistocene deglaciation based upon geophysical predictions of postglacial relative sea level change, *J. geophys. Res.,* **96,** 4497–4523.

Tushingham, A.M. & Peltier, W.R., 1992. Validation of the ICE-3G model of Würm–Wisconsin deglaciation using a global data base of relative sea level histories, *J. geophys. Res.,* **97,** 3285–3304.

Vacher, P., Mocquet, A. & Sotin, C., 1998. Computation of seismic profiles from mineral physics: the importance of the non-olivine components for explaining the 660 km depth discontinuity, *Phys. Earth planet. Inter.,* **106,** 275–298.

Verhoogen, J., 1965. Phase changes and convection in the earth's mantle, *Phil. Trans. R. Soc. Lond.,* A., **258,** 276–283.

Wahr, J. & Davis, J., 2002. Geodetic constraints on glacial isostatic adjustment, *Glacial Isostatic Adjustment and the Earth System: Sea Level, Crustal Deformation, Gravity and Rotation,* Vol. 103, eds Mitrovica, J. & Vermeersen, B., in press, AGU.

Wu, P., 1990. Deformation of internal boundaries in a viscoelastic Earth and topographic coupling between the mantle and core, *Geophys. J. Int.,* **101,** 213–231.

Wu, P. & Peltier, W.R., 1982. Viscous gravitational relaxation, *Geophys. J. R. astr. Soc.,* **70,** 435–485.

Yoder, C.F., Williams, J.H., Dickey, J.O., Schutz, B.E., Eanes, R.J. & Tapley, B.D., 1983. Secular variations of the Earth's gravitational harmonic J_2 coefficient from Lageos and nontidal acceleration of Earth rotation, *Nature,* **303,** 757–762.